Bioorganic Chemistry 104 (2020) 104198

Contents lists available at ScienceDirect

Bioorganic Chemistry

journal homepage: www.elsevier.com/locate/bioorg

Design and synthesis of some barbituric and 1,3-dimethylbarbituric acid derivatives: A non-classical scaffold for potential PARP1 inhibitors

Essam Eldin A. Osman[a,*], Noura S. Hanafy[b], Riham F. George[a], Samir M. El-Moghazy[a]

[a] Pharmaceutical Chemistry Department, Faculty of Pharmacy, Cairo University, Cairo 11562, Egypt
[b] Department of Pharmaceutical Chemistry, Faculty of Pharmacy, Heliopolis University for Sustainable Development, Cairo 11777, Egypt

ARTICLE INFO

Keywords:
Barbituric acid
PARP1 inhibitors
Molecular docking
MDA-MB-436

ABSTRACT

Six series based on barbituric acid **5a-e**, **10a-d**; thiobarbituric acid **6a-e**, **11a-d** and 1,3-dimethylbarbituric acid **7a-e**, **12a-d** were prepared and screened for their *in vitro* PARP1 inhibition. They revealed promising inhibition at nanomolar level especially compounds **5c**, **7b**, **7d** and **7e** (IC_{50} = 30.51, 41.60, 41.53 and 36.33 nM) with higher potency than olaparib (IC_{50} = 43.59 nM). Moreover, compounds **5b**, **5d**, **7a**, **12a** and **12c** exhibited good comparable activity (IC_{50} = 65.93, 58.90, 66.57, 45.40 and 50.62 nM, respectively). Furthermore, the most active compounds **5c**, **7b**, **7d**, **7e**, **12a** and **12c** against PARP1 *in vitro* were evaluated in the BRCA1 mutated triple negative breast cancer cell line MDA-MB-436 where **5c** and **12c** showed higher potency compared to olaparib and result in cell cycle arrest at G2/M phase. **5c** and **12c** showed apoptotic effects in MDA-MB-436 and potentiated the cytotoxicity of temozolomide in A549 human lung epithelial cancer cell line. Compounds **5c** and **12c** represent interesting starting points towards PARP1 inhibitors.

1. Introduction

Poly (ADP-ribose) polymerases (PARPs) is a big family comprised of 18 members involved in a number of cellular processes including surveillance of genome integrity, cell cycle checkpoints, DNA repair signaling pathways, apoptosis, and transcription [1–4]. PARP1 is the most abundant and well-characterized member among this family [1]. It is an important component of DNA damage response (DDR) that work to repair the DNA damage manifested as single strand DNA break (SSB) or double strand DNA break (DSB) and thus maintaining the cellular genomic stability [5]. More specifically, PARP1 is a cornerstone in the base excision repair (BER) with potential involvement in nucleotide excision repair (NER) mechanisms that provides repairment of SSB in eukaryotic cells [3,6]. Simply, the impaired DNA activates PARP1 to cleave its substrate nicotinamide adenine dinucleotide (NAD+) and transfer ADP-ribose units to nuclear target proteins to recruit BER components to facilitate DNA repair subsequently [4]. Thus, PARP inhibitors were suggested to enhance the cytotoxic effects of alkylating agents or radiation [7]. Moreover, homologous recombination (HR) and non-homologous end joining (NHEJ) are the two major mechanisms that cope with DSBs where the breast cancer–associated genes BRCA1 and BRCA2 are known to play an important role in HR [8–11]. BRCA1/2 deficient cells display impaired HR and high dependency on the activity of PARP leading to subsequent genomic instability [12,13]. PARP inhibition compromises SSB repair and BER, and in cells lacking intact HR mechanisms (BRCA1/2 mutants), the SSD are then converted into DSB, resulting in cell lethality [10,12–14]. Therefore, PARP inhibitors lead to what is known as “synthetic lethality” whereby DNA repair mechanisms are functionally shut down, causing cell death due to accumulation of genetic damage and PARP inhibitors were found to be toxic particularly in BRCA1/2 mutated cancer cell lines and human tumors [12–14]. In addition, BRCA1 mutation seems to be significantly overlapping in patients with “triple negative” breast cancer (TNBC) with deficiencies in the expression of estrogen receptor α (ER) and progesterone receptor (PR), and the HER2 gene [15].

More than 50% of BRCA1 carriers have TNBC. TNBC account for ~15% of the total diagnosed breast cancer cases with higher likelihood of recurrence and death [15].

Since nicotinamide (**I**) and 3-aminobenzamide (**II**) were identified as PARP1 inhibitors in the 1980s, great efforts have been devoted to discovering many structurally diverse PARP1 inhibitors [4,14,16–18]. Olaparib (AZD-2281, **III**), rucaparib (AG014699, **IV**) and niraparib (MK4827, **V**) have been approved by the FDA for the treatment of ovarian cancer in patients with or without BRCA mutations during the period of 2014–2017 and many other PARP1 inhibitors are being evaluated in different phases of clinical trials [18–21]. All these inhibitors are NAD analogues featuring a benzamide structure with common pharmacophoric features: carboxamide moiety and an

* Corresponding author.
E-mail address: essam.osman@pharma.cu.edu.eg (E. Eldin A. Osman).

https://doi.org/10.1016/j.bioorg.2020.104198
Received 2 June 2020; Received in revised form 26 July 2020; Accepted 17 August 2020
Available online 28 August 2020

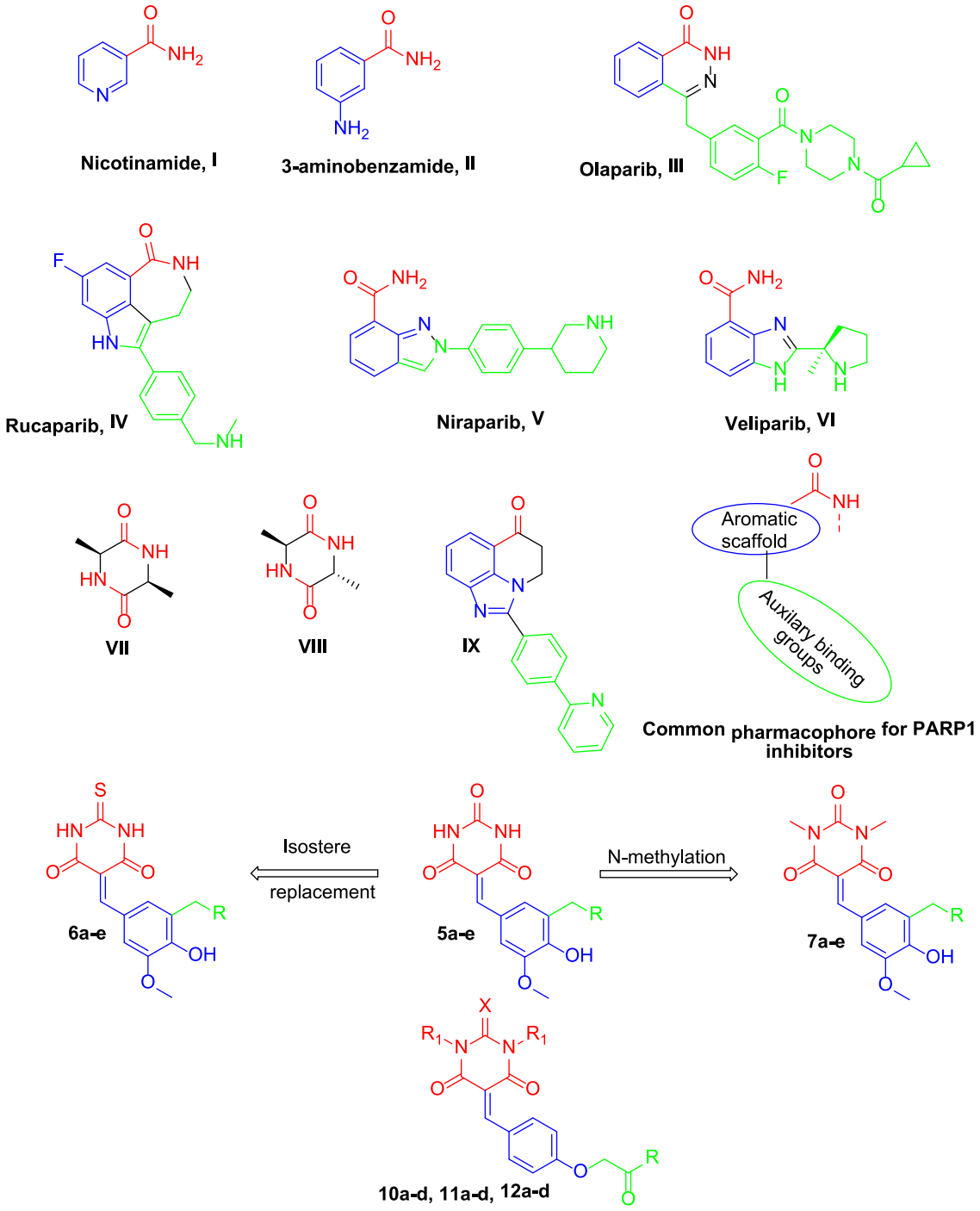

Fig. 1. Structure of select PARP1 inhibitors along with general pharmacophore for PARP1 inhibitors and the structure of the proposed compounds.

aromatic scaffold substituted with hydrophobic tail. This carboxamide moiety was either embedded into a lactam ring as in olaparib (**III**) and rucaparib (**IV**) or rotationally constrained by virtue of an intramolecular hydrogen bond forming a "pseudoring" as in niraparib (**V**) and veliparib (**VI**) (Fig. 1) [4]. Literature survey revealed various scaffolds for promising PARP1 inhibitors comprised of these common pharmacophoric features [4,18,22–27]. Based on several crystal structures and molecular modeling studies, the carboxamide functionality in these inhibitors was engaged in a network of hydrogen bonds with Gly863 and Ser904 in the nicotinamide binding subpocket [4]. Aromatic or unsaturated structures of the inhibitors form π stacking interactions with Tyr907 and in some cases with Tyr896 [4]. The back wall of the nicotinamide subpocket is lined by Ala898 and Lys903 forming a tight pocket capable of accommodating small substituents (e.g., CH_3, F, Cl) on the aromatic ring of the benzamide structures [4]. In some instances, Glu988 also formed a hydrogen bond with the inhibitors either directly or bridged through a conserved water molecule [4]. Lastly, a large hydrophobic subpocket adjacent to the nicotinamide binding often referred to as the adenine-ribose binding site is where most of PARP1 inhibitors take advantage to improve potency, solubility, and other pharmaceutical properties [4]. Recently, the natural 2,5-diketopiperazines (cyclic dipeptides) **VII**, **VIII**, lacking the common aromatic moiety in NAD+ competitive PARP1 inhibitors, were shown to inhibit the enzyme by virtue of the interaction with the key residues of the PARP1 active site [28]. As demonstrated using docking and molecular dynamics simulations one of the amide groups of cyclo(L-Ala-

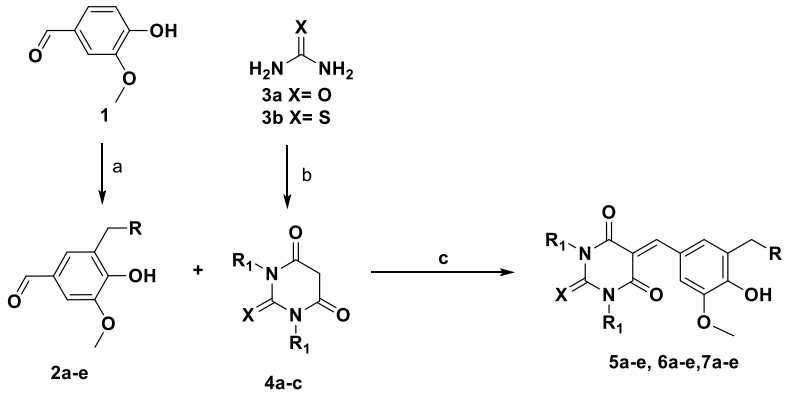

2a, R= Diethylamino
2b, R= Pyrrolidinyl
2c, R= Piperidinyl
2d, R= Morpholinyl
2e, R= 4-Methylpiperazinyl

4a, R_1=H, X= O
4b, R_1=H, X= S
4c, R_1=CH_3, X= O

5a, R= Diethylamino, R_1=H, X= O
5b, R= Pyrrolidinyl , R_1=H, X= O
5c, R= Piperidinyl, R_1=H, X= O
5d, R= Morpholinyl, R_1=H, X= O
5e, R= 4-Methylpiperazinyl, R_1=H, X= O
6a, R= Diethylamino, R_1=H, X= S
6b, R= Pyrrolidinyl,R_1=H, X= S
6c, R= Piperidinyl, R_1=H, X= S
6d, R= Morpholinyl, R_1=H, X= S
6e, R= 4-Methylpiperazinyl, R_1=H, X= S
7a, R= Diethylamino, R_1=CH_3, X= O
7b, R= Pyrrolidinyl,R_1=CH_3 X= O
7c, R= Piperidinyl, R_1=CH_3 X= O
7d, R= Morpholinyl, R_1=CH_3 X= O
7e, R= 4-Methylpiperazinyl, R_1=CH_3 X= O

Reagents and conditions
a) formaldehyde, appropriate secondry amine, ethanol 96%, reflux 30 min then stir at rt, 2h
b) diethylmalonate, Na metal, ethanol, reflux, 7h
c) absolute ethanol, reflux, 2h

Scheme 1. Synthetic pathway for preparation of target compounds **5a-e**, **6a-e** and **7a-e.**

L-Ala) **VII** and cyclo(L-Ala-D-Ala) **VIII** forms hydrogen bonds with Gly863, while the second amide group can form a hydrogen bond with Glu988, and one methyl group was having hydrophobic contact with Ala898 (Fig. 1S) [28]. Despite their weak affinity, these diketopiperazine inhibitors represent a promising basic structure for the design of more effective inhibitors of PARP family enzymes [28]. The non-selective PARP1/2 tricyclic benzimidazole, BYK236864, **IX** is another example of non-classical inhibitor lacking the lactam moiety and thus the hydrogen bond donor capability prevalent in so many NAD+ competitive inhibitors [29]. Based on the previous findings, barbituric acid moiety was postulated as a novel scaffold that could mimic the diketopiperazines for potential PARP1 inhibition. The diketopiperazine derivatives **VII**, **VIII** and barbituric acid were docked into the X-ray crystal structure of the active site of PARP1 in complex with olaparib (PDB: 5DS3) [30] to guide the design process (Fig. 1S-4S). Despite its slightly lower binding score (S = −4.68894053) compared to the diketopiperazine derivatives (S = -5.32370043 for **VII** and S = −5.35989285 for **VIII**), barbituric acid was forming the key hydrogen bonds with Gly863 and Ser904 and interestingly was able to stack to Tyr907 by virtue of its relatively planner structure (Fig. 4S). Next, we thought of extending the structure of barbituric acid at C5 which has reactive acidic hydrogen atoms (pKa = 4.01) [31]. Thus, 5-benzylidene derivative of barbituric acid was expected to increase the binding affinity through additional hydrophobic and π stacking interactions with Tyr896. Docking of the 5-benzylidene barbituric acid agreed with the previous hypothesis (S = −5.57461023) (Fig. 5S). An interesting notion was that the energy minimized structure of 5-benzylidene barbituric acid was predicted computationally to exist majorly as the barbituric acid mono anion (82.7%) at physiological pH. This mono anion would result in flipping of the compound in such a way that the barbiturate moiety would be oriented towards the opposite side of the binding pocket resulting in decreased inhibitory activity. Based on molecular modeling studies and calculation of the major ionized species at the physiological pH, grafting a phenolic group was predicted to suppress the ionization of the barbituric acid moiety to its conjugate base (51.9% vs 82.7%). 5-(4'-hydroxybenzylidene) barbituric acid docked nicely to the PARP1 active site and showed a relatively different binding mode of the phenyl ring where it was oriented away from the adenine binding pocket with its phenoxide ion forming a hydrogen bond with Met890 backbone NH with a slight decrease in the docking score compared to the non-phenolic derivative (S = −5.48069048) (Fig. 6S). 3'-methoxy substitution and auxiliary appendage with alkylamino methyl moieties were predicted to restore the binding mode towards adenosine subpocket with proposed interactions with Leu877, Arg878, Ile879, and Pro881 (Fig. 7S) providing the bases for the design of barbituric acid derivatives **5a-e**. Moreover, the design of other compounds relied on structure diversification of **5a-e** derivatives to allow useful structure activity relationship information through firstly isostere replacement of 2-oxo with sulfur atom in compounds **6a-e** since this may increase the lipophilicity of the compounds and afford better physicochemical properties. Secondly, substitution of the amide hydrogens with methyl groups in **7a-e** with the assumption that these compounds would have higher lipophilicity and would allow to orient the barbiturate moiety towards the nicotinamide binding pocket and may participate in hydrophobic bonding interactions with Ala898. Additionally, a longer tail attached to the aromatic core was introduced in compounds barbituric acid derivatives **10a-d**, thiobarbituric acid derivatives **11a-d** and 1,3-dimethylbarbituric acid derivatives **12a-d** to study the effects of these structural modifications on the biological activity. All the target compounds were screened for their PARP1 inhibitory activity and for their antiproliferative activity in the NCI 60 cell line screen. Furthermore, compounds eliciting promising PARP1 inhibition were screened for their cytotoxicity against the BRCA1 mutated triple negative breast cancer (TNBC) cell line MDA-MB-436. The

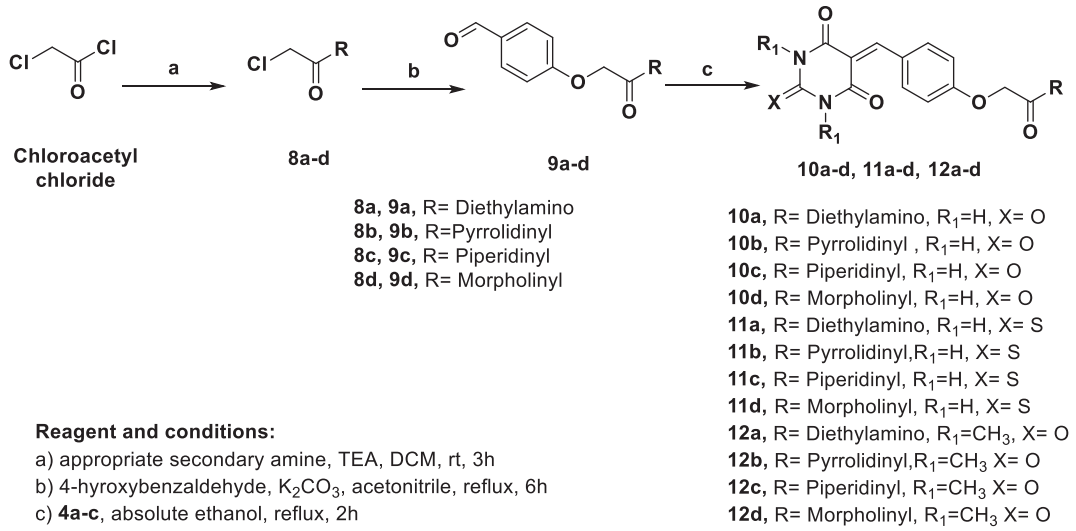

Scheme 2. The synthetic pathway for preparation of compounds **10a-d**, **11a-d** and **12a-d**.

effects of the most active compounds on the cell cycle of MDA-MB-436 cell line was investigated using flow cytometry. Potentiation of antiproliferative activity of temozolomide by the most active compounds was reported and molecular docking study was performed to shed light on the binding features essential for their activity.

2. Results and discussion

2.1. Chemistry

The steps followed for the synthesis of the key intermediates and the final compounds are summarized in Schemes 1 and 2. The functionalized aldehydes **2a-e** were prepared as reported by Mannich reaction of vanillin **1** with different secondary amines and 37% formaldehyde [32]. Furthermore, the reaction of urea **3a** or thiourea **3b** with diethylmalonate in ethanol in the presence of sodium ethoxide afforded as reported barbituric **4a** or thiobarbituric acid **4b**, respectively [33]. Knoevenagel condensation of aldehyde derivatives **2a-e** on the active methylene of **4a-c** in ethanol resulted in formation of **5a-e**, **6a-e** and **7a-e**, respectively (Scheme 1). Microanalyses and spectral data confirmed the structure of the synthesized compounds. The IR spectra of **5a-e** and **6a-e** showed the presence of OH, 2NH and C═O stretching band at 3422–3383, 3232–3182 and 1728–1670 cm^{-1}, while in case of compounds **6a-e**, an additional band appeared at 1192–1180 due to C═S. ^{1}H NMR charts showed characteristic signals at δ = 1.06–3.80 ppm assignable for diethylamino, pyrrolidinyl, piperidinyl, morpholinyl, piperazinyl protons. In addition, two singlets at 3.61–3.95 and 3.80–4.06 ppm attributed to NCH_2 and the methoxy protons, respectively along with singlet signals at δ = 7.72–9.48, 9.74–10.04, 11.40–11.47 and 11.53–11.58 ppm attributed to methylidene proton, OH and 2NH protons, respectively. ^{13}C NMR of compound **5a** was also consistent with the assigned structure where signals appeared at 11.8, 51.2 ppm assigned to ethyl carbons in addition to signals at 54.0, 56.2 ppm attributed to NCH_2 and OCH_3carbons, respectively along with signals at 91.8–147.0, 151.2, 164.2 and 165.4 ppm due to aromatic, olefinic carbons and 3carbonyl groups. Similarly, ^{13}C NMR spectrum of **5d** revealed signals at 52.6 and 65.7 ppm attributed to morpholine carbons in addition to signals at 56.2 and 57.6 ppm due to NCH_2 and OCH_3, respectively along with aromatic, olefinic carbons and three C = O at 91.7–147.3, 150.8 and 164.5 ppm. Moreover, the postulated structures of compounds **7a-e** were proved by the appearance of OH band and C═O in the IR spectra at 3441–3290 and 1724–1662 cm^{-1}, respectively. ^{1}H NMR spectra revealed the presence of three singlet signals at 2.98–3.43, 3.80–4.06 and 3.89–4.37 ppm corresponding to the $2CH_3$, NCH_2 and OCH_3 protons, respectively along with the aliphatic signals assigned to diethylamino, pyrrolidine-1-yl, piperidin-1-yl, morpholin-4-yl and 1-methylpiperazin-4-yl protons. In addition, a singlet signal appeared at 8.13–8.45 ppm assigned to methylidene proton with the D_2O exchangeable singlet signal at 9.70–12.70 ppm attributed to OH protons.^{13}C NMR of **7c** exhibited signals at 23.4, 25.2, 25.5 and 53.5 ppm due to piperidine carbons along with CH_2N carbon at 61.1 ppm in addition to signals appeared at 56.0, 151.6, 159.1 and 164.7 ppm due to OCH_3 group and three C = O. Furthermore, ^{13}C NMR of compound **7d** displayed morpholine carbons at 52.7 and 66.5 ppm in addition to signals at 28.4, 29.1, 56.1 and 61.0 ppm due to two CH_3, OCH_3 and NCH_2 carbons, respectively. Furthermore, acylation of the appropriate secondary amine with chloroacetyl chloride was achieved in dry DCM in the presence of triethylamine as HCl scavenger to obtain compounds **8a-d** as reported [34]. The reaction of the latter with *p*-hydroxybenzaldehyde in dry acetonitrile in the presence of potassium carbonate resulted in formation of **9a-d**.[34]. Then, condensation of the aldehyde derivatives **9a-d** with the appropriate barbituric acid **4a-c** in ethanol afforded the target compounds **10a-d**, **11a-d** and **12a-d**, respectively (Scheme 2). The expected structures of compounds **10a-d** were confirmed by IR spectra that displayed characteristic vibration bands in the range of 3221–3132 and 1743–1661 cm^{-1}attributed to the NH and C═O, respectively. ^{1}H NMR spectra revealed a singlet signal of the methylene protons (-O-C$\underline{H}_2$-C═O) at 4.87–5.00 ppm, in addition to another aliphatic signals at 1.01–3.60 ppm due to the secondary amine protons. Also, a singlet signal appeared at 8.19–8.23 ppm corresponding to the methylidene protons(–C = C$\underline{H}$) along with two D_2O exchangeable singlet signals assigned to the 2NH group appeared at 9.08–11.27 ppm. ^{13}C NMR of compound **10d** exhibited signals at 45.0 and 66.1 ppm due to morpholine carbons along with OCH_2 carbon at 66.5 ppm in addition to the signals corresponding to the aromatic and olefinic carbons at 114.6–156.0 ppm and 4C = O signals at 150.7, 162.6, 164.4 and 165.9 ppm. Additionally, IR spectra of **11a-d** demonstrated the appearance of the characteristic stretching vibration bands of the amidic NH, C═O and C═S groups at 3190–3116, 1700–1661 and 1226–1215 cm^{-1}, respectively. ^{1}H NMR spectra of compounds **11a-d** revealed aliphatic signals assignable for diethylamino, pyrrolidinyl, piperidinyl, morpholinyl protons at 1.05–3.61 ppm, together with a singlet signal at 4.61–5.01 ppm due to OCH_2 in addition to the appearance of aromatic doublet signals at 6.68–8.37 ppm corresponding to the inserted phenyl moiety along with the singlet signal at 8.20–8.32 ppm assigned to the methylidene proton. In addition to the appearance of D_2O exchangeable singlet signals around 11.35–12.35 ppm corresponding to the two NH protons.^{13}C NMR of

compound **11a** revealed signals at 14.2, 14.6 and 41.1, 41.3 ppm assigned to diethyl carbons along with signals at 66.7 ppm due to methylene carbon. Furthermore, ^{13}C NMR of compound **11c** displayed piperidine carbons at 24.1, 25.6, 26.2, 42.9 and 45.6 ppm in addition to signal at 66.1 ppm due to CH_2 carbon.^{13}C NMR of **11d** exhibited signals at 41.0 and 61.5 due to morpholine carbons along with OCH_2 carbon at 63.0 ppm. IR spectra of **12a-d** revealed the presence of stretching C═O around 1732–1661 cm^{-1}. ^{1}H NMR showed the appearance of a sharp singlet signal around 3.38–3.41 ppm corresponding to the protons of two methyl groups together with an extra singlet signal at 4.72–4.79 ppm assigned for the methylene group in addition to signals attributed to the aliphatic secondary amine protons at 1.13–3.74 ppm. Moreover, three signals appeared in the aromatic region, two doublet signals at 7.01–7.02 and 8.28–8.30 ppm assigned for aromatic protons and one singlet signal at 8.49–8.50 ppm due to the methylidene proton.^{13}C NMR spectrum of **12b** revealed signals at 23.8, 25.9, 45.3 and 46.2 ppm attributed to pyrrolidine carbons in addition to signals at 28.3 and 66.2 ppm due to CH_3 and CH_2 carbons. Moreover, ^{13}C NMR spectrum of compound **12c** revealed signals at 24.3, 25.5, 26.4, 43.1 and 46.1 ppm assigned to piperidine carbons along with signal at 67.0 ppm due to methylene carbon in addition to signals at 28.9 and 29.0 ppm due to two methyl carbons.

2.2. Biological evaluation

2.2.1. PARP1 inhibitory activity and structure activity relationship

All the synthesized compounds were tested in PARP1 inhibitory assay *in vitro* using olaparib as a reference standard. The PARP1 inhibitory activities as IC_{50} (nM) against PARP1 are presented in Table 1. The target pyrimidinones **5a-e, 6a-e, 7a-e** exhibited a wide range of PARP1 inhibitory activity but all in the nanomolar range with IC_{50} values in the range of 30–265 nM. The piperidine derivative **5c** was the most active compound among the barbituric acid derivatives **5a-e**. The order of activity was piperidino > morpholino > pyrrolidino > diethylamino > methylpiperazino. It is worth to mention that **5c** displayed the highest activity among all the target compounds (IC_{50} = 30.51 nM) and even higher than the reference drug olaparib (IC_{50} = 43.59 nM). The thiobarbituric acid derivatives **6a-e** displayed much lower potency compared to their oxygen counterparts **5a-e**. The diminished activity of **6a-e** might be justified by the weaker hydrogen bonding capability of the thioxo group (electronic and/or steric features) or the lower solubility of this series. Only the methylpiperazino derivative **6e** showed appreciable activity among this series (IC_{50} = 72.37 nM) and the order of activity was methylpiperazino > piperidino > diethylamino > pyrrolidino > morpholino. Generally, the 1,3-dimethylbarbituric acid derivatives **7a-e** exhibited the highest activity among all the pyrimidinone compounds. Compounds **7b** and **7d** were nearly equipotent. Moreover, compound **7e** displayed the highest activity among this series (IC_{50} = 36.33 nM). Concerning the 4-alkylaminoacetoxy derivatives **10a-d, 11a-d** and **12a-d**, the target compounds exhibited a wide range of PARP1 inhibitory activity with IC_{50} in the range of 45–667 nM. Regarding the 5-benzylidenepyrimidinone derivatives **10a-d** (barbituric acid derivatives) and the 5-bezylidene-2-thioxodihydropyrimidinone **11a-d** (thiobarbituric acid derivatives), a comparison between the two series revealed that **11a-d** displayed lower activity than **10a-d** series. Moreover, barbituric acid derivatives **10a-d** showed less inhibitory activity relative to the standard olaparib (IC_{50} = 43 nM). For the compounds bearing 1,3-dimethylbarbituric moiety **12a-d**, introduction of two methyl groups on the barbituric acid ring increased the inhibitory activity. The order of activity was diethylamino > piperidino > morpholino > pyrrolidino. Moreover, pyrrolidino **12b** and morpholino **12d** derivatives were nearly equipotent (IC $_{50}$ = 91.70 and 90.03 nM, respectively). It is worth to mention that compound **12a** showed higher potency (IC_{50} = 45.40 nM) being nearly equivalent to **12c**

Table 1

In vitro inhibitory activity of the synthesized compounds against PARP1.[a]

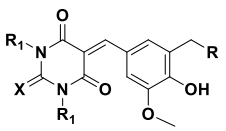

5a-e: R_1=H, X =O
6a-e: R_1=H, X =S
7a-e: R_1=CH_3, X =O

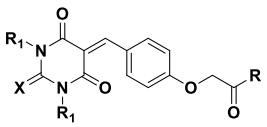

10a-d: R_1=H, X =O
11a-d: R_1=H, X =S
12a-d: R_1=CH_3, X =O

Compd. ID.	R	IC_{50} (nM) ± SD.	Compd. ID.	R	IC_{50} (nM) ± SD.
5a		204.35 ± 4.62	**7e**	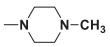	36.33 ± 0.92
5b		65.93 ± 1.41	**10a**		244.05 ± 7.23
5c		30.51 ± 8.71	**10b**		197.30 ± 6.28
5d		58.90 ± 1.73	**10c**		111.62 ± 2.84
5e	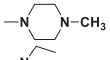	204.72 ± 6.03	**10d**		98.28 ± 2.71
6a		102.26 ± 1.57	**11a**		131.27 ± 4.13
6b		229.61 ± 6.85	**11b**		310.08 ± 8.41
6c		96.73 ± 2.44	**11c**		667.56 ± 17.1
6d		265.90 ± 6.59	**11d**		136.77 ± 3.85
6e	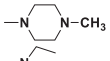	72.37 ± 1.82	**12a**		45.40 ± 1.61
7a		66.57 ± 2.4	**12b**		91.70 ± 3.25
7b		41.60 ± 1.26	**12c**		50.62 ± 13.08
7c		84.22 ± 2.1	**12d**		90.03 ± 4.36
7d		41.53 ± 1.35	**Olaparib**	–	43.59 ± 1.37

[a] Values are means from three independent dose–response curves.

Table 2
The results of the target compounds in the NCI-60 human tumor cell lines screen.

Compound	NSC Number	% Mean Growth	Delta	Range
5a	805279	103.66	17.94	28.65
5b	805277	105.95	19.52	42.37
5c	805274	106.01	17.07	32.29
5d	805273	106.61	22.05	38.62
5e	805280	104.68	21.74	35.61
6a	805282	106.66	16.52	31.44
6b	805278	105.06	18.03	32.47
6c	805276	102.96	42.18	60.10
6d	805275	105.40	18.71	29.83
6e	805281	106.54	21.24	43.14
7a	814336	100.45	25.37	40.92
7b	814335	100.66	73.23	86.50
7c	814333	99.84	24.39	40.71
7d	814334	101.29	23.12	34.12
7e	814337	102.32	20.28	33.54
10a	821612	105.52	15.47	26.42
10b	821611	104.07	24.50	51.59
10c	821613	105.24	16.57	33.54
10d	821614	104.49	20.13	44.19
11a	821602	100.16	24.63	37.62
11b	821601	98.75	18.16	29.85
11c	821603	100.24	15.58	28.22
11d	821604	100.71	17.46	31.22
12a	821607	105.47	15.72	28.93
12b	821606	99.28	26.77	39.35
12c	821608	105.54	17.34	35.67
12d	821609	105.16	18.55	36.00

(IC_{50} = 50.62 nM). In summary, the most active compounds were **5c, 7b, 7d, 7e, 12a** and **12c**. Based on these findings, barbituric acid and 1,3-dimethylbarbituric acid could potentially serve as successful scaffolds for potential PARP1 inhibitors. Moreover, belonging of the active compounds to different series suggested that a wide variety of molecular fragments can be tolerated in the tail portion of the molecule.

2.2.2. NCI-60 human tumor cell lines screen

All the compounds were screened at the National Cancer Institute (NCI), USA for their antiproliferative activity at a single dose of 10 μM using sulforhodamine B assay (SRB). The results are shown in Table 2. All the compounds showed no toxicity in the tested cell lines. This was not surprising, since none of these cell lines harbor BRCA1/2 mutations with the exception of non-deleterious BRCA1 mutation in the ovarian cell lines IGROV-1 and OVCAR8 and four variants of BRCA2 identified in three microsatellite unstable (MSI+) colon carcinoma cell lines of the NCI-60 (HCT-116, HCT-15 and KM12) [35,36]. BRCA2 has not been reported as a cancer gene (either a susceptibility gene or somatically mutated) in colon cancer and somatic mutations of BRCA2 are generally very rare [35]. The presence of heterozygous truncating variants of BRCA2 in HCT-15, KM12, and HCT-116 was suggested to be due to the microsatellite instability of the cell lines and do not contribute to tumorigenesis [35]. Olaparib (NSC: 747856 and 753686) showed almost no growth inhibition at 10 μM in the NCI-60 human tumor cell lines screen with an average GI_{50} of 46.1 μM against the whole panel of the cell lines and GI_{50} of 100 μM against the BRCA2 mutated cell lines HCT-116, HCT-15 and KM12. Furthermore, the activity profile of the tested compounds in the NCI-60 human tumor cell lines screen is suggestive of the lack of any nonspecific reactivity.

2.2.3. Antiproliferative activity against BRCA1 mutated cell line MDA-MB-436

As some PARP inhibitors have been shown to display single agent activity for tumors lacking BRCA1/2 dependent DNA double-stranded repair mechanisms [8,10]. Therefore, compounds exhibited promising PARP1 inhibition comparable to olaparib namely **5c, 7b, 7d, 7e, 12a** and **12c** were investigated for their potential antiproliferative activity against BRCA1 mutated cell line MDA-MB-436. This assay was performed at VACSERA, Egypt and the results are summarized in Table 3. MDA-MB-436 cell line is a triple negative breast cancer cell line that had the 5396 + 1G > A mutation in the splice donor site of exon 20 with two identified transcript lengths [37]. The 5396 + 1G > A mutation has been reported 46 times in the BIC mutation database and is classified as pathogenic [37]. The *in vitro* antiproliferative effects of the tested compounds against MDA-MB-436 cell line were variable despite their nearly equal IC_{50} against PARP1 *in vitro*. Moreover, most of the tested compounds showed moderate antiproliferative activities against MDA-MB-436 cell line with IC_{50} values ranging from 3.65 to 29.8 μM. Three compounds **5c, 7e** and **12c** exhibited enhanced antitumor activities compared to the standard olaparib (IC_{50} = 6.84 μM). Compounds **7b** and **7d** displayed moderate activity and compound **12a** showed weak activity. The most active compound was the barbituric acid derivative **5c** with IC_{50} = 3.65 μM and the 1,3-dimethylbarbituric acid derivative **12c** with IC_{50} = 3.73 ± 0.1 μM. The variability in the antiproliferative activity of the tested compounds may be attributed to variable physicochemical properties and solubilities that would affect membrane permeability.

Table 3
The antiproliferative activity (IC_{50}, μM) of the tested compounds against MDA-MB-436 cancer cell line.[a]

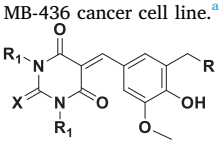

5a-e: R_1=H, X =O
7a-e: R_1=CH_3, X =O

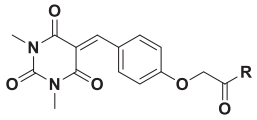

12a-d

Compound ID	R	IC_{50} (μM) ± SD
5c		3.65 ± 0.1
7b		13.2 ± 0.3
7d		10.4 ± 0.3
7e	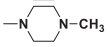	6.01 ± 0.2
12a		29.8 ± 0.8
12c		3.73 ± 0.1
Olaparib	–	6.84 ± 0.2

[a] Values are means from three independent dose–response curves.

2.2.4. Cell cycle analysis in MDA-MB-436 cells and apoptotic effects of 5c and 12c

The role of PARP1 inhibitors in induction of apoptosis is well documented [38–40]. Flow cytometry using Annexin V/PI double staining was performed on MDA-MB-436 cells incubated with **5c** or **12c** at two different concentrations: 1 μM and the IC_{50} concentration of each compound for 48 h. Flow cytometric analysis showed that **5c** and **12c** caused cell cycle arrest at G2/M phase with dose-dependent increases in the G2/M cell population and a significant increase in cells with a pre-G1 DNA content, suggestive of apoptosis, Fig. 2. This profile was consistent with previous reports demonstrating the same trend for PARP1 inhibitors [40–42]. Compounds **5c** and **12c** showed a definite concentration dependent apoptotic effect where the late apoptotic events were more significant as the concentration of the compound increased, Fig. 3.

2.2.5. Potentiation of temozolomide antiproliferative activity in A549 human lung cancer cells

Previous studies document the role of PARP1 inhibitors in sensitizing BRCA competent cell lines to DNA damaging agents as radiation and methylating agents [25,43,44]. Thus, compounds **5c** and **12c** were

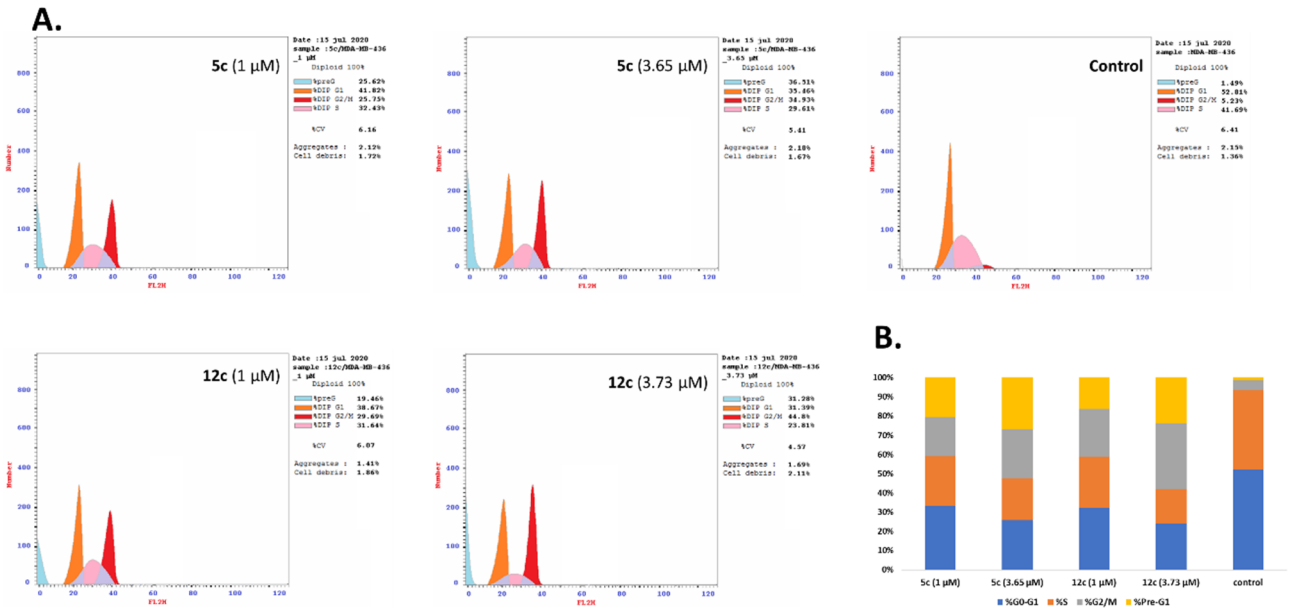

Fig. 2. **5c** and **12c** result in G2/M cell cycle arrest and increase Pre-G1 cell population in MDA-MB-436 cells. (A) Flow cytometric cell cycle analysis of MDA-MB-436 cells treated with **5c** or **12c**. (B) Quantification of the different cell cycle phases of MDA-MB-436 cells treated with **5c** and **12c.**

further tested for their potential to potentiate the antiproliferative effects of the DNA methylating agent temozolomide (TMZ) in a non BRCA mutated cell line using MTT assay, Fig. 4. A549 lung epithelial cancer cell line with competent DNA repair mechanism was selected based on previous reports [44,45]. TMZ is an alkylating agent whose cytotoxicity is based on methylation of N7 in guanine and formation of O6-methylguanine in DNA that induces single strand DNA breaks [44]. A549 cells showed low sensitivity to either olaparib or TMZ when used as a single agent (IC_{50} = 12.3 ± 0.69 and 24.2 ± 1.36 μM, respectively. While the barbituric acid derivative **5c** was even less effective (IC_{50} = 33.2 ± 1.86 μM), the 1,3-dimethylbarbituric acid derivative **12c** was the most active against A549 cells (IC_{50} = 7.94 ± 0.45 μM) as a single agent. Combination of TMZ with 0.5 μM of **5c**, **12c** or olaparib resulted in potentiating TMZ activity. TMZ potency when combined with 0.5 μM **12c** was about 7 times higher (IC_{50} = 3.64 ± 0.2 μM) compared to TMZ alone (IC_{50} 24.2 ± 1.36 μM). Combining olaparib (0.5 μM) with TMZ resulted in higher IC_{50} for TMZ (IC_{50} = 5.05 ± 0.28 μM) compared to **12c**. Finally, the barbituric acid derivative **5c**, potentiated the effect of TMZ in A549 cells (IC_{50} = 8.03 ± 0.45 μM) but to a lesser extent compared to either olaparib or **5c**. These results demonstrated that compounds **5c** and **12c** at 0.5 μM potentiated the antiproliferative effect of TMZ in A549 cell line and highlight the potential of **12c** for further in-depth analysis. Fig. 4.

2.3. Molecular docking study

Initially, molecular docking of the target compounds was performed at human PARP1 catalytic domain to support the design approach by comparing the binding scores and patterns of the designed compounds

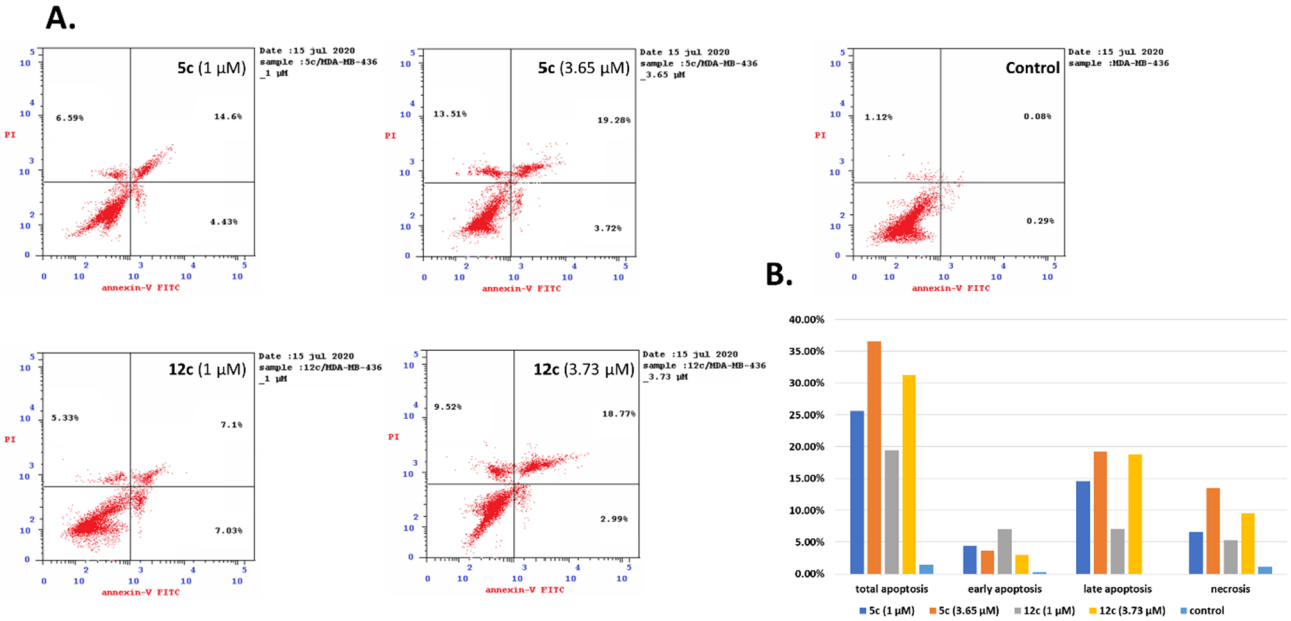

Fig. 3. **5c** and **12c** induce apoptosis in MDA-MB-436 cells. (A) PI/Annexin double staining for detection of apoptosis and necrosis. (B) Summary of the apoptotic and necrotic effects of **5c** and **12c** in MDA-MB-436 cells.

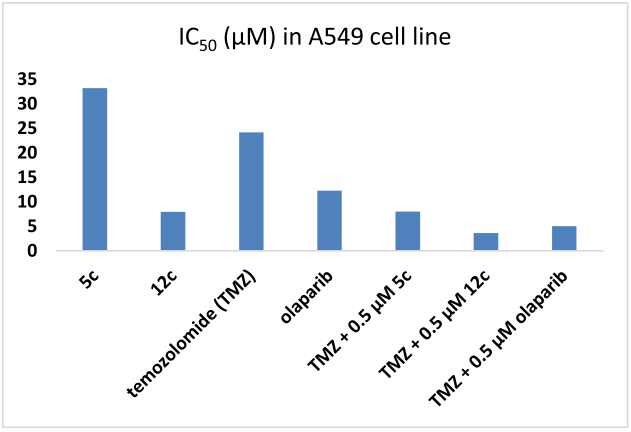

Fig. 4. 5c and **12c** potentiate the effect of DNA methylating agent temozolomide (TMZ) in A549 lung epithelial cancer cells. IC_{50} values are means from three independent experiments.

with that of the reference drug Olaparib using Molecular Operating Environment (MOE 10.2015) software provided by Chemical Computing Group, Canada [16]. Following the *in vitro* PARP1 inhibition assay, the docking results were reinspected to correlate and justify the biological activity. To ensure the accuracy of the docking protocol, validation was performed by re-docking of the co-crystallized ligand Olaparib into the PARP1 catalytic domain. The docking validation results showed perfect superimposition between the coordinates of Olaparib in the X-ray crystal structure and its self-docked pose with root mean square deviation (RMSD) of 0.514 and docking score (S) of −8.1 Kcal mol^{-1} (Fig. 8S). During the preparation of the compounds for docking we noticed that the nature of the secondary amine affects their major ionized species predicted at physiological pH and this was expected to affect the physicochemical properties of these compounds and consequently their binding interaction with PARP1 and their membrane permeability and pharmacokinetic profile. Compounds **5a-e**, **6a-e** and **7a-e** contain the phenol and secondary amine moieties that were predicted to exist majorly as zwitter ions where the secondary amines were protonated, and the phenol was existing as a phenoxide ion. The barbituric acid moiety in **5a-e** were existing as a mixture of non-ionized acid and the conjugate base nearly in the ratio of 2:1. For **6a-e**, no ionized forms were observed for the thiobarbituric acid given its weak acidity compared to barbituric acid and for **7a-e** as the acidic protons of barbituric acid were replaced by methyl groups. For compounds **10a-d**, **11a-d** and **12a-d**, the 3ry amides in the tail functionalities were not protonated since the nitrogen atom in these molecules were involved in resonance with the adjacent carbonyl group. Barbituric acid and thiobarbituric acid were > 90% existing as non-ionized forms in **10a-d** and **11a-d**, respectively. Compounds **12a-d** were exclusively existing in non-ionized forms since they contain no ionizable acidic nor basic groups. For the docking study, the major ionized form of each compound was considered for performing the docking experiment. Docking was performed using "Triangle Matcher" placement method, poses were prioritized based on London dG scoring function, refinement of the results was done using the default forcefield and the binding score (S) and amino acids interactions were recorded. Generally, the target compounds were binding the active site of PARP1 in accordance with the expected pharmacophore guided binding mode and the top docking poses of compounds of the most active compounds **5c, 7b, 7d, 7e, 12a** and **12c** were analyzed in more detail. Barbituric acid derivatives **5a-e** were generally making the crucial hydrogen bonding interactions with Gly863 and Ser904. Aromatic stacking with Tyr 907 was preserved in

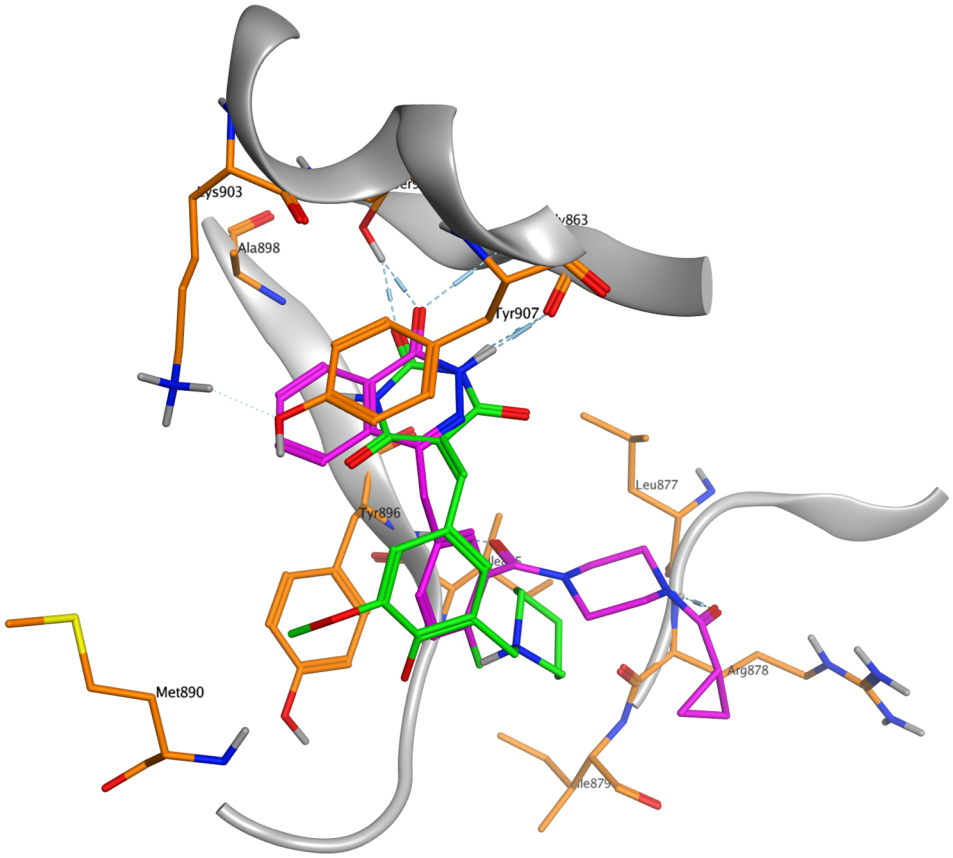

Fig. 5. The top docking pose of barbituric acid derivative **5c** (green) superimposed on olaparib (magenta) at the active site of PARP1 (PDB: 5DS3) (S = −7.2477994). (For interpretation of the references to color in this figure legend, the reader is referred to the web version of this article.)

all the top docking poses and the benzylidene stacking to Tyr 896 was recorded in some poses. The benzylidene moiety and the amine part of the tail functionality were oriented towards the adenosine binding subpocket in all the docking poses. Hydrogen bonds to Arg878 were sometimes observed in addition to other favourable hydrophobic interactions with the side chains of amino acids Leu877, Ile879, Ala880 and Pro881. It is worthy to mention that the interaction of these amine tails could be optimized by extending the structure through a longer tail as in compounds **10a-d**, **11a-d** and **12a-d**. The top docking pose of the barbituric acid piperidine derivative **5c** is shown in Fig. 5.

While most of the top docking poses of compounds **10a-d** revealed the placement of the barbituric acid moiety towards the NAD+ binding subpocket, some poses were flipped where this moiety was oriented close to the adenine binding subpocket and this may justify for their lower binding affinities. The docking results agreed with the fact that thiobarbituric acid derivatives **6a-e** and **11a-d** were showing lower binding affinities to PARP1 *in vitro*. We correlate this to the weaker hydrogen bonding capabilities of these derivatives, Fig. 6.

Interestingly, the dimethylbarbituric acid moieties in **7a-e** and **12a-d** containing no hydrogen bond donor were having the highest score in our docking study despite binding in a different manner compared to their non methylated counterparts **5a-e** and **10a-d.** Taking compounds **7e**, **12a** and **12c** as an example (Figs. 7–9), the steric hinderance elicited by the methyl groups made the interaction of the carbonyl group at C2 with Gly863 and/or Ser904 impossible. Alternatively, one of the carbonyl groups at C4 or C6 were the donor of the recorded hydrogen bond to Gly863 and/or Ser904. Interestingly, C2 carbonyl was engaged in some dipole or hydrogen bond interaction with Lys903. Tyr907 was still forming the stacking interaction with the dimethylbarbituric acid and one of the methyl groups was found nicely fitting the tight hydrophobic pocket close to Ala898 while the other was facing the solvent front near Glu988. No correlation between the nature of the amine within the same series and the binding score was observed, suggesting that the major contributing factor for the differences in the *in vitro* binding assay was related to differences in physicochemical properties of these compounds (ionization and/or solubilities) and consequently their binding interaction with PARP1. This may affect their membrane permeability and consequently their cellular effects in MDA-MB-436 cancer cell line.

3. Conclusion

Based on molecular modeling, a series of 5-benzylidene barbituric acid derivatives were designed and synthesized as potential non classical PARP1 inhibitors. The synthesized compounds were featuring barbituric acid in **5a-e** and **10a-d**, thiobarbituric acid in **6a-e** and **11a-d** or 1,3-dimethylbarbituric acid in **7a-e** and **12a-d**. The benzylidene moieties were functionalized with 3-methoxy, 4-hydroxy and 5-alkylaminomethyl groups in **5a-e, 6a-e** and **7a-e** or 4-alkylaminoacetoxy groups in **10a-d, 11a-d** and **12a-d.** The synthesized compounds showed variable inhibitory activity but all in the nanomolar range with IC_{50} in the range of 30.5–667.5 nM against PARP1 *in vitro* compared to the reference standard olaparib (IC_{50} = 43.6 nM). Barbituric derivatives **5a-e** and **10a-d** showed superior inhibitory activity compared to their thioxo counterparts **6a-e** and **11a-d** emphasizing the importance of hydrogen bonding capability of the carbonyl group in PARP1 inhibitors. Only the piperidinomethyl derivative **5c** (IC_{50} = 30.5 nM) was more potent compared to olaparib. Interestingly, the 1,3-dimethylbarbituric acid derivatives **7a-e** were among the most active compounds possibly due to the hydrophobic interaction of one of its methyl groups with Ala898 at PARP1 active site. The pyrrolidinomethyl derivative **7b** was more potent and **7d** and **7e** were equipotent compared to olaparib. The 4-alkylaminoacetoxy derivatives **10a-d** and **11a-d** were less potent than olaparib and their 3-methoxy, 4-hydroxy, 5-alkylaminomethyl counterparts **5a-e** and **6a-e.** The 5-(4-alkylaminoacetoxy-benzylidene)-1,3-dimethylbarbituric acid derivatives **12a** and **12c** were more or less equipotent compared to olaparib. The nature of the amine tail within the same series of compounds was predicted using molecular modeling study to affect the ionization states of these derivatives but was not correlated with the observed *in vitro* activity as well as their docking scores. All the compounds showed no antiproliferative activity in the NCI 60 cell line screening assay at 10 μM and that was in accordance

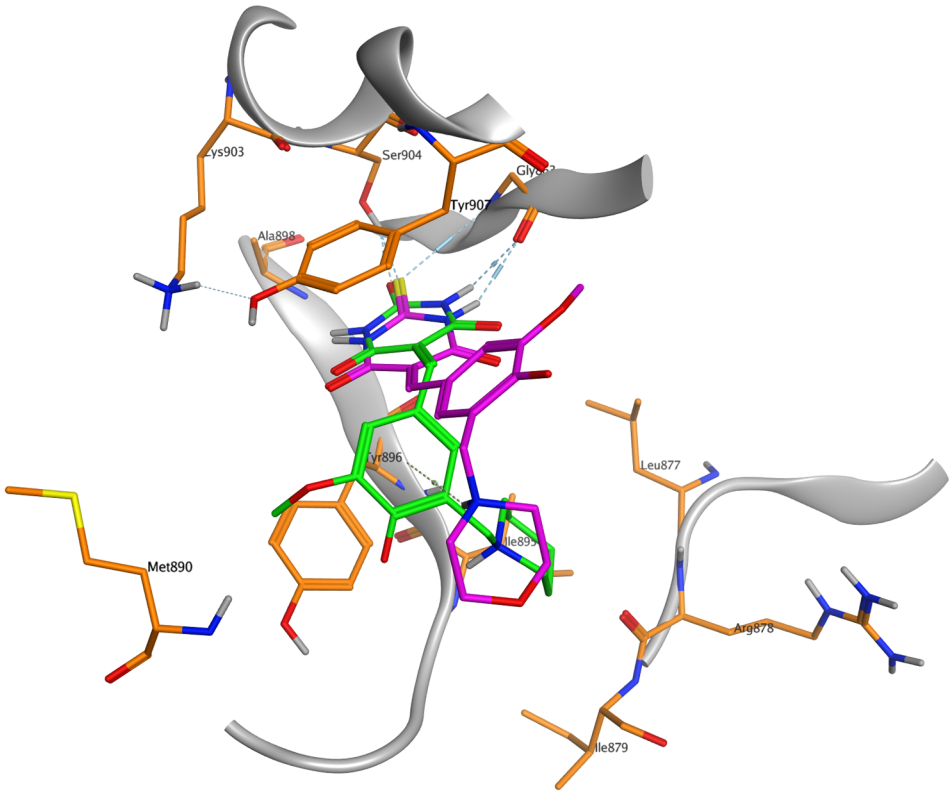

Fig. 6. The top docking pose of the thiobarbituric acid derivative **6d** (magenta) (S = −6.07522392) superimposed on barbituric acid derivative **5c** (green) (S = −7.2477994) at the active site of PARP1 (PDB: 5DS3). (For interpretation of the references to color in this figure legend, the reader is referred to the web version of this article.)

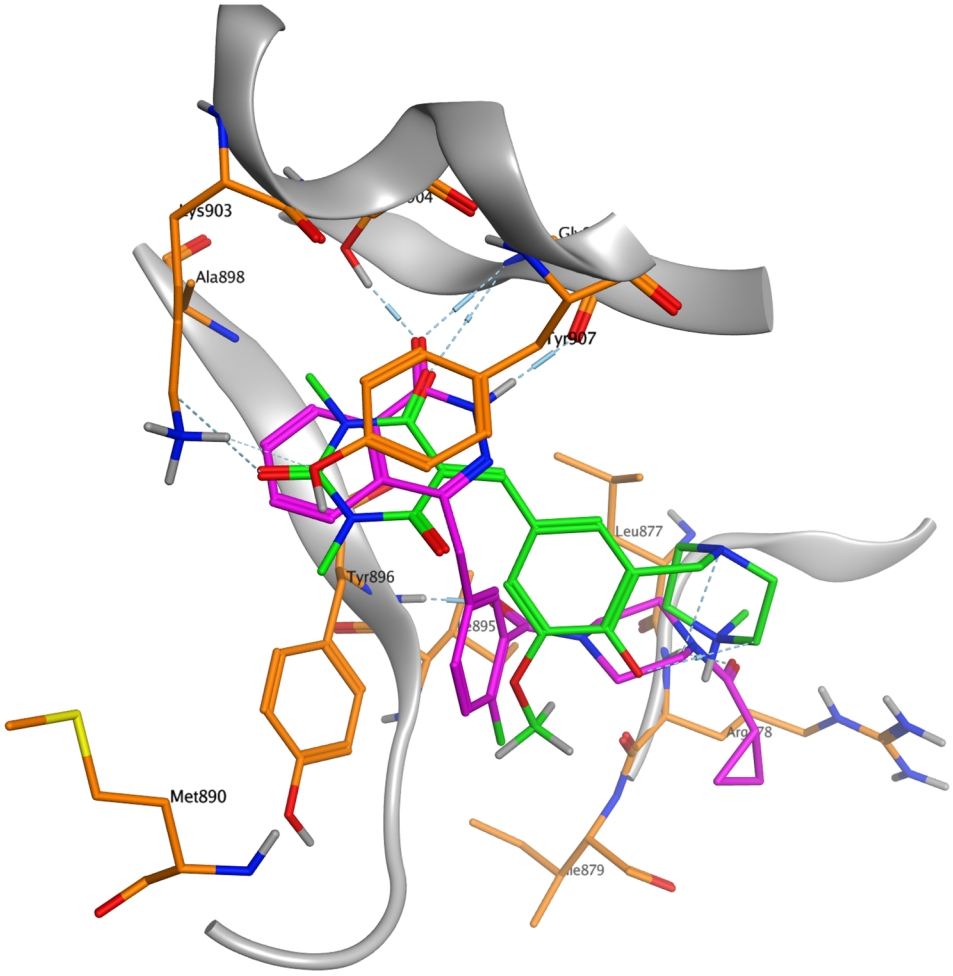

Fig. 7. . The top docking pose of the 1,3-dimethylbarbituric acid derivative **7e** (green) (S = −7.75939894) superimposed on olaparib (magenta) at the active site of PARP1 (PDB: 5DS3). (For interpretation of the references to color in this figure legend, the reader is referred to the web version of this article.)

with the absence of the BRCA1/2 mutation in these cell lines. The most active compounds **5c**, **7b**, **7d**, **7e**, **12a** and **12c** against PARP1 *in vitro* were further evaluated in the BRCA1 mutated triple negative breast cancer cell line MDA-MB-436 where **5c** and **12c** were twice more potent compared to olaparib and **7e** was slightly more potent. **5c** and **12c** caused cell cycle arrest at G2/M phase in MDA-MB-436 cell line and induced apoptosis. These compounds at 0.5 µM potentiated the antiproliferative effect of the DNA methylating agent temozolomide in BRCA1 competent A549 lung epithelial cancer cell line. The different cellular activity of the tested compounds in MDA-MB-436 cell line despite their nearly PARP1 enzymatic inhibitory activity points out to the effect of their physicochemical properties as ionization and solubility on membrane permeability. Further studies will be conducted to optimize these properties in a separate study.

4. Experimental

4.1. Chemistry

Melting points were determined by open capillary tube method using Electrothermal 9100 melting point apparatus MFB-595-010 M (Gallen Kamp, London, England) and are uncorrected. Microanalyses were carried out at The Regional Center for Mycology and Biotechnology, Al-Azhar University. Infrared spectra were recorded at Micro Analytical Center, Faculty of pharmacy, Cairo University as potassium bromide discs on Schimadzu FT-IR 8400S spectrophotometer (Shimadzu, Kyoto, Japan) and expressed in wave number υ_{max} (cm^{-1}). ^1H NMR and ^{13}C NMR were recorded at Micro-analytical Center, Faculty of Pharmacy, Cairo University on Bruker spectrophotometer at 400 MHz using tetramethylsilane (TMS) as internal reference. Chemical shift values (δ) are given in parts per million (ppm). Some spectra were performed on nmr 400 mercury 400 spectrometer. TLC was performed on TLC plates UV fluorescent silica gel (60 FZSU) and were visualized using UV lamp. Compounds **2a-e** [32], **4a,b** [33], **8a-d** [34] and **9a-d** [34] were prepared according to their reported procedures.

4.1.1. General procedure for preparation of *5a-e, 6a-e and 7a-e*

A mixture of equimolar amounts of **2a-e** and **4a-c** (1 mmol) in absolute ethanol (15 ml) was heated under reflux for 2 h. The formed precipitate was filtered, dried and recrystallized from ethanol.

*4.1.1.1. 5-(3-((Diethylamino)methyl)-4-hydroxy-5-methoxybenzylidene) pyrimidine-2,4,6 (1H,3H,5H)-trione **(5a)***. It was prepared from **2a** (0.24 g, 1 mmol) and **4a** (0.13 g, 1 mmol) to give (0.25 g, yield: 70%); m.p.>300 °C; IR ν (cm^{-1}): 3417 (OH), 3232 (2NH), 1685,1670 (3C=O); ^1H NMR (400 MHz, DMSO-d_6, δ, ppm): 1.06 (t, J = 7.20 Hz, 3H, CH_3 of diethylamine), 1.19 (t, J = 7.20 Hz, 3H, CH_3 of diethylamine), 2.60 (q, J = 7.20 Hz, 2H, CH_2 of diethylamine), 2.90 (q, J = 7.20 Hz, 2H, CH_2 of diethylamine), 3.74 (s, 2H, NCH_2), 3.80 (s, 3H, OCH_3), 7.14 (s, 1H, ArH), 7.31 (s, 1H, ArH), 9.48 (s, 1H, -C=CH–), 9.64 (s, 1H, OH, D_2O exchangeable), 13.46 (s, 2H, NH, D_2O exchangeable); ^{13}C NMR (100 MHz, DMSO-d_6, δ, ppm): 11.8 (CH_3 of diethylamine), 51.2 (CH_2 of diethylamine), 54.0 (NCH_2), 56.2 (OCH_3), 91.8, 111.0, 120.8, 125.7, 130.4, 135.3, 143.3, 147.0 (Ar and olefinic Cs), 151.2, 164.2, 165.4

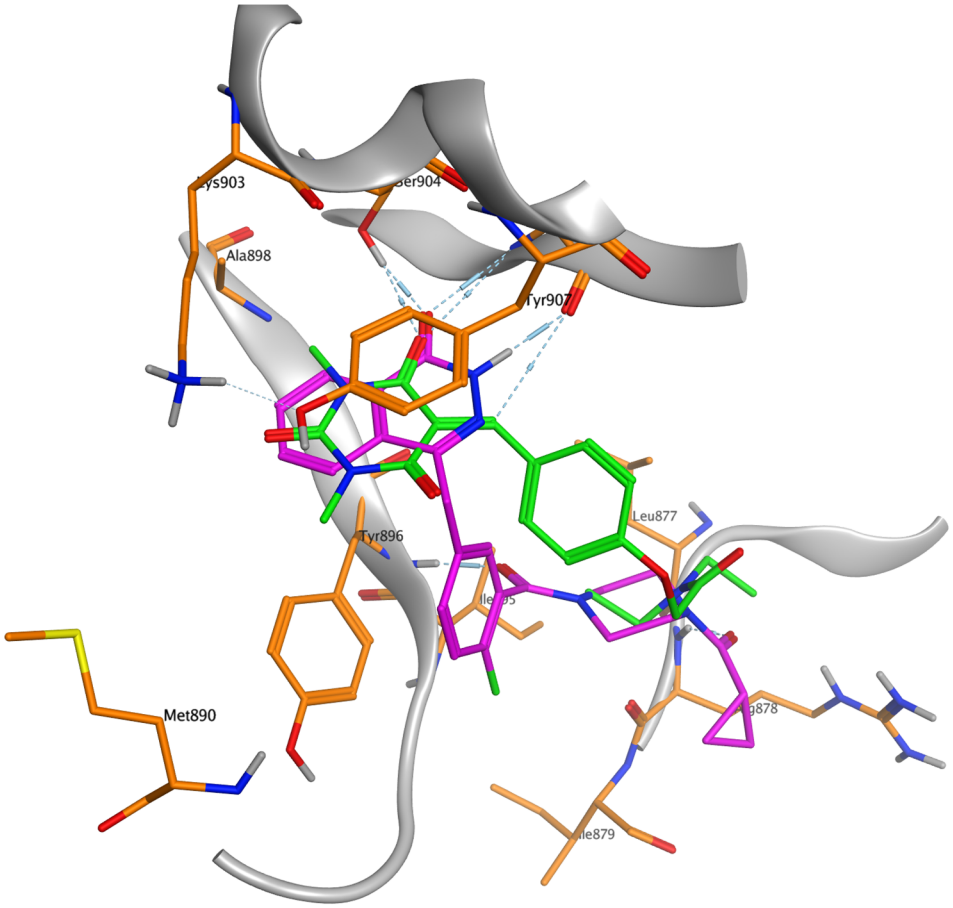

Fig. 8. The top docking pose of the 1,3-dimethylbarbituric acid derivative **12a** (green) (S = −7.61911821) superimposed on olaparib (magenta) at the active site of PARP1 (PDB: 5DS3). (For interpretation of the references to color in this figure legend, the reader is referred to the web version of this article.)

(3C═O); Anal. calcd. for $C_{17}H_{21}N_3O_5$; C, 58.78; H, 6.09; N, 12.10; Found; C, 59.06; H, 6.23; N, 12.36.

4.1.1.2. 5-(4-Hydroxy-3-methoxy-5-(pyrrolidin-1-ylmethyl)benzylidene) pyrimidine-2,4,6 (1H,3H,5H)-trione ***(5b)***. It was prepared from **2b** (0.24 g, 1 mmol) and **4a** (0.13 g, 1 mmol) to give (0.25 g, yield: 85%); m.p.>300 °C; IR ν (cm^{-1}): 3421 (OH), 3194 (2NH), 1728, 1678 (3C═O); ^{1}H NMR (400 MHz, DMSO-d_6, δ, ppm): 1.82–1.91 (m, 4H, $2CH_2$ pyrrolidine), 3.16 (brs, 4H, $N(CH_2)_2$ pyrrolidine), 3.95 (s, 2H, NCH_2) 4.06 (s, 3H, OCH_3), 7.76 (s, 1H, ArH), 7.88 (s, 1H, ArH), 8.58 (s, 1H, -C═CH–), 10.04 (s, 1H, OH, D_2O exchangeable), 10.48 (s, 2H, NH, D_2O exchangeable); Anal. calcd. for $C_{17}H_{19}N_3O_5$; C, 59.12; H, 5.55; N, 12.17; Found; C,59.35; H,5.67; N,12.41.

4.1.1.3. 5-(4-Hydroxy-3-methoxy-5-(piperidin-1-ylmethyl)benzylidene) pyrimidine-2,4,6(1H,3H,5H)-trione ***(5c)***. It was prepared from **2c** (0.25 g, 1 mmol) and **4a** (0.13 g, 1 mmol) to give (0.30 g, yield: 83%); m.p.>300 °C; IR ν (cm^{-1}): 3421 (OH), 3182 (2NH), 1725, 1716 (3C═O); ^{1}H NMR (400 MHz, DMSO-d_6, δ, ppm): 1.49–1.69 (m, 6H, $3CH_2$ piperidine), 2.96 (brs, 4H, $N(CH_2)_2$ piperidine), 3.64 (s, 2H, NCH_2), 3.98 (s, 3H, OCH_3), 7.75 (s, 1H, ArH), 7.93 (s, 1H, ArH), 8.55 (s, 1H, -C═CH–), 10.02 (s, 1H, OH, D_2O exchangeable), 10.59 (s, 2H, NH, D_2O exchangeable); ^{13}C NMR (100 MHz, DMSO-d_6, δ, ppm): 22.2, 23.2, 25.3 (piperidine $3CH_2$), 52.2 ($N(CH_2)_2$ piperidine), 55.2 (–OCH_3), 56.5 (–CH_2N), 102.8, 115.7, 117.4, 119.9, 142.0, 143.9, 147.2, 149.9 (Ar and olefinic Cs), 151.1, 153.2, 170.9 (3C═O); MS, *m/z* [%]: 359.06 [M^+, 100]; Anal. calcd. for $C_{18}H_{21}N_3O_5$; C, 60.16; H, 5.89; N, 11.69; Found; C, 60.38; H, 5.97; N, 11.88.

4.1.1.4. 5-(4-Hydroxy-3-methoxy-5-(morpholinomethyl)benzylidene) pyrimidine-2,4,6(1H,3H,5H)-trione ***(5d)***. It was prepared from **2d** (0.25 gm, 1 mmol) and **4a** (0.13 g, 1 mmol) to give (0.29 g, yield: 81%); m.p.>300 °C; IR ν (cm^{-1}): 3422 (OH), 3209 (2NH), 1739, 1674 (3C═O); ^{1}H NMR (400 MHz, DMSO-d_6, δ, ppm): 2.66 (brs, $N(CH_2)_2$ morpholine), 3.67 (brs, 4H, $O(CH_2)_2$ morpholine), 3.86 (s, 2H, NCH_2), 3.91 (s, 3H, OCH_3), 7.80 (s, 1H, ArH), 8.16 (s, 1H, ArH), 8.46 (s, 1H, -C═CH–), 9.98 (s, 1H, OH, D_2O exchangeable), 11.07 (br s, 1H, NH, D_2O exchangeable), 11.15 (br s, 1H, NH, D_2O exchangeable); ^{13}C NMR (100 MHz, DMSO-d_6, δ, ppm): 52.6 ($N(CH_2)_2$ morpholine), 56.0 (–OCH_3), 57.6 (–CH_2N), 65.7 ($O(CH_2)_2$ morpholine), 91.7, 112.6, 121.3, 122.6, 134.9, 135.8, 143.3, 147.3 (Ar and olefinic Cs), 150.8, 164.5 (3C═O); Anal. calcd. for $C_{17}H_{19}N_3O_6$; C, 56.51; H, 5.30; N, 11.63; Found; C, 56.79; H, 5.46; N, 11.80

4.1.1.5. 5-(4-Hydroxy-3-methoxy-5-((4-methylpiperazin-1-yl)methyl) benzylidene) pyrimidine-2,4,6 (1H,3H,5H)-trione ***(5e)***. It was prepared from **2e** (0.26 gm, 1 mmol) and **4a** (0.13 g, 1 mmol) to give (0.21 g, yield: 56%); m.p. 268–270 °C; IR ν (cm^{-1}): 3422 (OH), 3197 (2NH), 1701, 1681 (3C═O); ^{1}H NMR (400 MHz, DMSO-d_6, δ, ppm): 2.43 (s, 3H, NCH_3), 3.32–3.38 (m, 8H, $2N(CH_2)_2$ methylpiperazine), 3.74 (s, 2H, NCH_2), 3.83 (s, 3H, OCH_3), 7.15 (s, 1H, ArH), 7.32 (s, 1H, ArH), 7.72 (s, 1H, -C═CH–), 9.74 (s, 1H, OH, D_2O exchangeable), 10.04 (s, 2H, NH, D_2O exchangeable); Anal. calcd. for $C_{18}H_{22}N_4O_5$; C, 57.75; H, 5.92; N, 14.96; Found; C, 58.01; H, 6.14; N, 14.75.

4.1.1.6. 5-(3-((Diethylamino)methyl)-4-hydroxy-5-methoxybenzylidene)-2-thioxodihydropyrimidine −4,6(1H,5H)-dione ***(6a)***. It was prepared from **2a** (0.24 g, 1 mmol) and **4b** (0.14 g, 1 mmol) to give (0.20 g, yield: 56%); m.p. > 300 °C; IR ν (cm^{-1}): 3421 (OH), 3197 (2NH), 1678 (2C═O), 1184 (C═S); ^{1}H NMR (400 MHz, DMSO-d_6, δ, ppm):

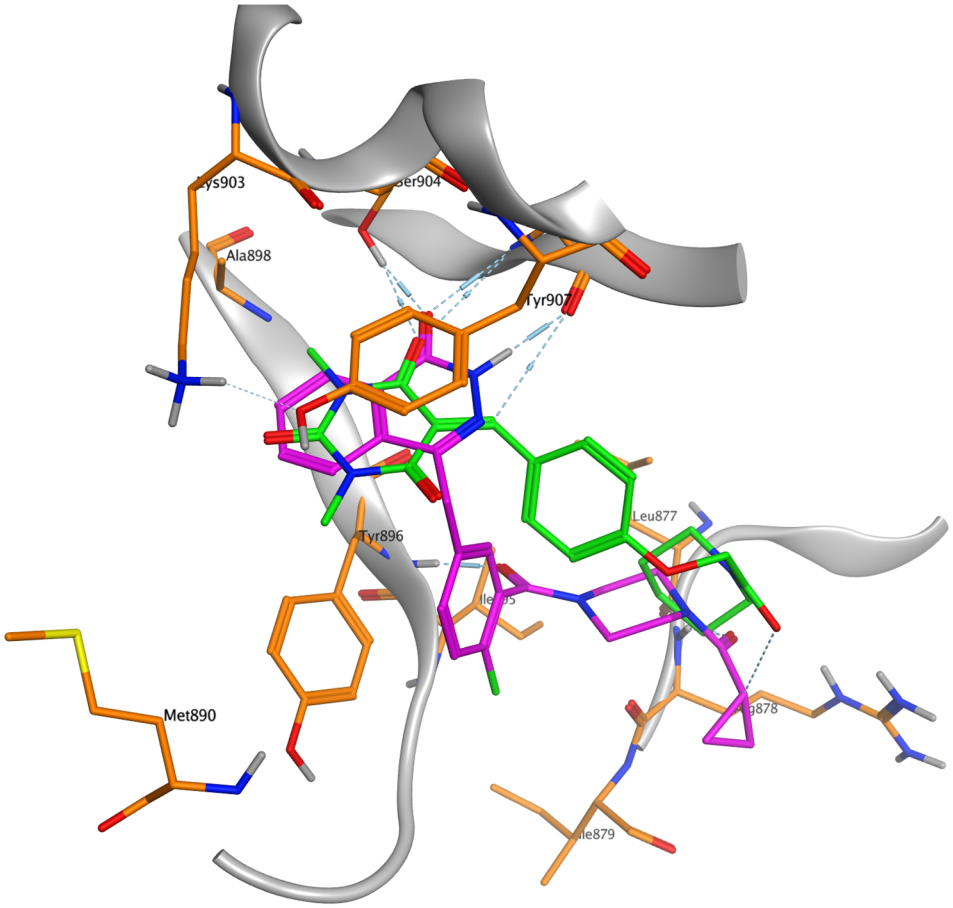

Fig. 9. The top docking pose of the 1,3-dimethylbarbituric acid derivative **12c** (green) (S = −7.69142628) superimposed on olaparib (magenta) at the active site of PARP1 (PDB: 5DS3). (For interpretation of the references to color in this figure legend, the reader is referred to the web version of this article.)

1.16–1.25 (m, 6H, $2CH_3$ of diethylamine), 2.94–3.06 (m, 4H, $2CH_2$ of diethylamine), 3.70 (s, 2H, NCH_2), 4.05 (s, 3H, OCH_3), 6.62 (s, 1H, ArH), 7.83 (s, 1H, ArH), 8.51 (s, 1H, -C═CH–), 10.62 (s, 1H, OH, D_2O exchangeable), 11.45 (s, 1H, NH, D_2O exchangeable), 11.58 (s, 1H, NH, D_2O exchangeable); MS, *m/z* [%]: 361.46 [M^+, 8.48]; Anal. calcd. for $C_{17}H_{21}N_3O_4S$; C, 56.18; H, 5.82; N, 11.56; Found; C, 56.36; H, 5.94; N, 11.80.

4.1.1.7. 5-(4-Hydroxy-3-methoxy-5-(pyrrolidin-1-ylmethyl)benzylidene)-2-thioxodihydropyrimidine −4,6(1H,5H)-dione ***(6b)***. It was prepared from **2b** (0.24 g, 1 mmol) and **4b** (0.14 g, 1 mmol) to give (0.24 g, yield: 67%); m.p.>300 °C; IR ν (cm^{-1}): 3402 (OH), 3186 (2NH), 1678 (2C═O), 1180 (C═S); ^1H NMR (400 MHz, DMSO-d_6, δ, ppm): 1.84 (br s, 4H, $2CH_2$ pyrrolidine), 3.02 (brs, 4H, $N(CH_2)_2$ pyrrolidine), 3.75 (s, 2H, NCH_2), 3.99 (s, 3H, OCH_3) , 6.60 (s, 1H, ArH), 7.12 (s, 1H, ArH), 8.43 (s, 1H, -C═CH–), 10.92 (s, 1H, OH, D_2O exchangeable), 11.47 (s, 2H, NH, D_2O exchangeable); Anal. calcd. for $C_{17}H_{19}N_3O_4S$; C, 56.50; H, 5.30; N, 11.63; Found; C, 56.82; H, 5.43; N, 11.76.

4.1.1.8. 5-(4-Hydroxy-3-methoxy-5-(piperidin-1-ylmethyl)benzylidene)-2-thioxodihydropyrimidine-4,6(1H,5H)-dione ***(6c)***. It was prepared from **2c** (0.25 g, 1 mmol) and **4b** (0.14 g, 1 mmol) to give (0.23 g, yield: 60%); m.p. > 300 °C; IR ν (cm^{-1}): 3394 (OH), 3197 (2NH), 1671 (2C═O), 1180 (C═S); ^1H NMR (400 MHz, DMSO-d_6, δ, ppm): 1.47–1.63 (m, 6H, $3CH_2$ piperidine), 3.04–3.13 (m, 4H, $N(CH_2)_2$ piperidine), 3.66 (s, 2H, NCH_2), 4.00 (s, 3H, OCH_3), 6.58 (s, 1H, ArH), 7.13 (s, 1H, ArH), 8.35 (s, 1H, -C═CH–), 10.88 (s, 1H, OH, D_2O exchangeable), 11.41 (s, 1H, NH, D_2O exchangeable), 11.56 (s, 1H, NH, D_2O exchangeable); Anal. calcd. for $C_{18}H_{21}N_3O_4S$; C, 57.58; H, 5.64; N, 11.19; Found; C, 57.81; H, 5.78; N, 10.95.

4.1.1.9. 5-(4-Hydroxy-3-methoxy-5-(morpholinomethyl)benzylidene)-2-thioxodihydropyrimidine-4,6(1H,5H)-dione ***(6d)***. It was prepared from **2d** (0.25 g, 1 mmol) and **4b** (0.14 g, 1 mmol) to give (0.22 g, yield: 59%); m.p. > 300 °C; IR ν (cm^{-1}): 3402 (OH), 3209 (2NH), 1681 (2C═O), 1192 (C═S); ^1H NMR (400 MHz, DMSO-d_6, δ, ppm): 2.85 (brs, 4H, $N(CH_2)_2$ morpholine), 3.73–3.80 (m, 6H, $O(CH_2)_2$morpholine and NCH_2), 3.83 (s, 3H, OCH_3), 6.57 (s, 1H, ArH), 7.34 (s, 1H, ArH), 8.34 (s, 1H, -C═CH–), 10.87 (s, 1H, OH, D_2O exchangeable), 11.40 (s, 1H, NH, D_2O exchangeable), 11.53 (s, 1H, NH, D_2O exchangeable); Anal. calcd. for $C_{17}H_{19}N_3O_5S$; C, 54.10; H, 5.07; N, 11.13; Found; C, 54.32; H, 5.21; N, 11.40.

4.1.1.10. 5-(4-Hydroxy-3-methoxy-5-((4-methylpiperazin-1-yl)methyl) benzylidene)-2-thioxodihydropyrimidine-4,6(1H,5H)-dione ***(6e)***. It was prepared from **2e** (0.26 g, 1 mmol) and **4b** (0.14 g, 1 mmol) to give (0.24 g, yield: 62%); m.p. 275–277 °C; IR ν (cm^{-1}): 3383 (OH), 3197 (2NH), 1670 (2C═O), 1180 (C═S); ^1H NMR (400 MHz, DMSO-d_6, δ, ppm): 2.43 (m, 3H, CH_3), 2.83 (br s, 4H, $N(CH_2)_2$methylpiperazine), 3.42 (brs, 4H, $N(CH_2)_2$methylpiperazine), 3.61 (s, 2H, NCH_2), 3.86 (s, 3H, OCH_3), 6.49 (s, 1H, ArH), 7.36 (s, 1H, ArH), 7.81 (s, 1H, -C═CH–), 9.78(s, 1H, OH, D_2O exchangeable), 11.43 (s, 1H, NH, D_2O exchangeable), 11.55 (s, 1H, NH, D_2O exchangeable); Anal. calcd. for $C_{18}H_{22}N_4O_4S$; C, 55.37; H, 5.68; N, 14.35; Found; C, 55.46; H, 5.89; N, 14.52.

4.1.1.11. 5-(3-((Diethylamino)methyl)-4-hydroxy-5-methoxybenzylidene)-1,3-dimethylpyrimidine-2,4,6(1H,3H,5H)-trione ***(7a)***. It was prepared from **2a** (0.24 g, 1 mmol) and **4c** (0.16 g, 1 mmol) to give (0.29 g, yield: 76%), m.p. > 300 °C; IR ν (cm^{-1}): 3441 (OH), 3051 (CH aromatic), 2978 (CH aliphatic), 1701 (3C═O); ^1H NMR

(400 MHz, $CDCl_3$, δ, ppm): 1.42–1.58 (m, 6H, $2CH_3$ of diethylamine), 3.34 (s, 6H, $2CH_3$), 3.40–3.46 (m, 4H, $2CH_2$ of diethylamine), 4.06 (s, 2H, NCH_2), 4.37 (s, 3H, OCH_3), 7.25 (s, 1H, ArH), 7.74 (s, 1H, ArH), 8.14 (s, 1H, -C═CH–), 12.70 (s, 1H, OH, D_2O exchangeable). Anal. calcd. for $C_{19}H_{25}N_3O_5$; C, 60.79; H, 6.71; N, 11.19; Found: C, 60.96; H, 6.89; N, 11.08.

4.1.1.12. 5-(4-Hydroxy-3-methoxy-5-(pyrrolidin-1-ylmethyl)benzylidene)-1,3-dimethylpyrimidine-2,4,6(1H,3H,5H)-trione ***(7b)***. It was prepared from **2b** (0.24 g, 1 mmol) and **4c** (0.16 g, 1 mmol) to give (0.24 g, yield: 64%); m.p.$^{>}$300 °C; IR ν (cm^{-1}): 3390 (OH), 3062 (CH aromatic), 2962 (CH aliphatic), 1682 (3C═O); ^{1}H NMR (400 MHz, $CDCl_3$, δ, ppm): 1.75–1.82 (m, 4H, $2CH_2$ pyrrolidine), 2.63–2.80 (m, 4H, N$(CH_2)_2$pyrrolidine), 2.98 (s, 6H, $2CH_3$), 3.80 (s, 2H, NCH_2), 3.89 (s, 3H, OCH_3), 6.36 (s, 1H, ArH), 7.29 (s, 1H, ArH), 8.13 (s, 1H, -C═CH–), 9.70 (s, 1H, OH, D_2O exchangeable); MS, *m/z* [%]: 375.26 [M^+, 27.21]; Anal. calcd. for $C_{19}H_{23}N_3O_5$; C, 61.12; H, 6.21; N, 11.25; Found; C, 60.98; H, 6.43; N, 11.49.

4.1.1.13. 5-(4-Hydroxy-3-methoxy-5-(piperidin-1-ylmethyl)benzylidene)-1,3-dimethylpyrimidine-2,4,6(1H,3H,5H)-trione ***(7c)***. It was prepared from **2c** (0.25 g, 1 mmol) and **4c** (0.16 g, 1 mmol) to give (0.30 g, yield: 76%); m.p. $^{>}$ 300 °C; IR ν (cm^{-1}): 3441 (OH), 3089 (CH aromatic), 2954 (CH aliphatic), 1708 (3C═O); ^{1}H NMR (400 MHz, $CDCl_3$, δ, ppm): 1.70–1.76 (m, 6H, $3CH_2$ piperidine), 2.68–2.73 (m, 4H, N$(CH_2)_2$ piperidine), 3.40 (s, 6H, $2CH_3$), 3.90 (s, 2H, NCH_2), 3.96 (s, 3H, OCH_3), 7.74 (s, 1H, ArH), 8.27 (s, 1H, ArH), 8.41 (s, 1H, -C═CH–), 9.77 (s, 1H, OH, D_2O exchangeable); ^{13}C NMR (100 MHz, DMSO-d_6, δ, ppm): 23.4, 25.2, 25.5 ($3CH_2$ piperidine), 28.5 ($2CH_3$), 53.5 (N$(CH_2)_2$ piperidine), 56.0 (–OCH_3), 61.1 (–CH_2N), 111.6, 117.5, 119.7, 122.8, 132.9, 148.0, 154.7, 158.1 (Ar and olefinic Cs), 151.6, 159.1, 164.7 (3C═O). Anal. calcd. for $C_{20}H_{25}N_3O_5$; C, 62.00; H, 6.50; N, 10.85; Found; C, 61.83; H, 6.42; N, 10.69.

4.1.1.14. 5-(4-Hydroxy-3-methoxy-5-(morpholinomethyl)benzylidene)-1,3-dimethylpyrimidine-2,4,6(1H,3H,5H)-trione ***(7d)***. It was prepared from **2d** (0.25 g, 1 mmol) and **4c** (0.16 g, 1 mmol) to give (0.35 g, yield: 89%); m.p. $^{>}$ 300 °C; IR ν (cm^{-1}): 3433 (OH), 3060 (CH aromatic), 2978–2939 (CH aliphatic), 1724, 1662 (3C═O); ^{1}H NMR (400 MHz, $CDCl_3$, δ, ppm): 2.68 (m, 4H, N$(CH_2)_2$ morpholine), 3.41 (s, 3H, CH_3), 3.42 (s, 3H, CH_3), 3.80 (br s, 4H, O$(CH_2)_2$morpholine), 3.87 (s, 2H, NCH_2), 3.98 (s, 3H, OCH_3), 7.70 (s, 1H, ArH), 8.29 (s, 1H, ArH), 8.43 (s, 1H, -C═CH–), 9.09 (s, 1H, OH, D_2O exchangeable); ^{13}C NMR (100 MHz, DMSO-d_6, δ, ppm): 28.4, 29.1 ($2CH_3$), 52.7 (N$(CH_2)_2$ morpholine), 56.1 (–OCH_3), 61.0 (NCH_2), 66.5 (O$(CH_2)_2$ morpholine), 113.4, 117.6, 119.9, 124.3, 131.9, 147.6, 154.1, 159.0 (Ar and olefinic Cs), 151.5, 161.2, 163.4 (3C═O); Anal. calcd. for $C_{19}H_{23}N_3O_6$; C, 58.60; H, 5.95; N, 10.79; Found; C, 58.54; H, 6.17; N, 10.58.

4.1.1.15. 5-(4-Hydroxy-3-methoxy-5-((4-methylpiperazin-1-yl)methyl) benzylidene) −1,3-dimethyl pyrimidine-2,4,6(1H,3H,5H)-trione ***(7e)***. It was prepared from **2e** (0.26 g, 1 mmol) and **4c** (0.16 g, 1 mmol) to give (0.34 g, yield: 85%); m.p. $^{>}$ 300 °C; IR ν (cm^{-1}): 3290 (OH), 3001 (CH aromatic), 2958–2939 (CH aliphatic), 1693, 1666 (3C═O); ^{1}H NMR (400 MHz, $CDCl_3$, δ, ppm): 2.40 (s, 3H, CH_3), 2.74 (brs, 4H, N$(CH_2)_2$ methylpiperazine), 3.33–3.34 (m, 4H, N$(CH_2)_2$ methylpiperazine), 3.41 (s, 3H, CH_3), 3.43 (s, 3H, CH_3), 3.86 (s, 2H, NCH_2), 3.98 (s, 3H, OCH_3), 7.69 (s, 1H, ArH), 8.30 (m, 1H, ArH), 8.45 (s, 1H, -C═CH–), 9.79 (s, 1H, OH, D_2O exchangeable); Anal. calcd. for $C_{20}H_{26}N_4O_6$; C, 59.69; H, 6.51; N, 13.92; Found; C, 59.91; H, 6.43; N, 14.05.

4.1.2. General procedure for preparation of ***10a-d, 11a-d*** *and* ***12a-d***

A mixture of **4a-c** and **9a-d** (1 mmol) in absolute ethanol (15 ml) was heated under reflux for 2hrs. The formed precipitate was filtered, dried and recrystallized from ethanol.

4.1.2.1. N,N-Diethyl-2-(4-((2,4,6-trioxotetrahydropyrimidin-5(2H)-ylidene) methyl) phenoxy) acetamide ***(10a)***. It was prepared from **4a** (0.13 g, 1 mmol) and **9a** (0.24 g, 1 mmol) to give (0.20 g, yield: 59%); m.p. $^{>}$ 300 °C; IR ν (cm^{-1}): 3132 (2NH), 3060 (CH aromatic), 2974–2935 (CH aliphatic), 1693 (4C═O); ^{1}H NMR (400 MHz, DMSO-d_6, δ, ppm): 1.01–1.21 (m, 6H, $2CH_3$ diethylamine), 3.12–3.34 (m, 4H, $2CH_2$ diethylamine), 4.93 (s, 2H, O-CH_2-C═O), 7.06 (d, J = 8.80 Hz, 2H, ArH), 7.83 (s, 1H, -C═CH–), 8.29 (d, J = 8.80 Hz, 2H, ArH), 9.84 (s, 1H, NH, D_2O exchangeable), 9.90 (s, 1H, NH, D_2O exchangeable); Anal. calcd. for $C_{17}H_{19}N_3O_5$ C, 59.12; H, 5.55; N, 12.17; Found; C, 59.36; H, 5.42; N, 12.38.

4.1.2.2. 5-(4-(2-Oxo-2-(pyrrolidin-1-yl)ethoxy)benzylidene)pyrimidine-2,4,6(1H,3H,5H)-trione ***(10b)***.. It was prepared from **4a** (0.13 g, 1 mmol) and **9b** (0.23 g, 1 mmol) to give (0.22 g, yield: 65%); m.p.$^{>}$300 °C; IR ν (cm^{-1}): 3194 (2NH), 3086 (CH aromatic), 2881 (CH aliphatic), 1720, 1690, 1680, 1666 (4C═O); ^{1}H NMR (400 MHz, DMSO-d_6, δ, ppm): 1.73–1.91 (m, 4H, $2CH_2$ pyrrolidine), 3.41–3.46 (m, 4H, N$(CH_2)_2$ pyrrolidine), 4.87 (s, 2H, OCH_2-C═O), 6.86 (d, J = 8.80 Hz, 2H, ArH), 8.19 (s, 1H, -C═CH–), 8.31 (d, J = 8.80 Hz, 2H, ArH), 11.09 (s, 1H, NH, D_2O exchangeable), 11.22 (s, 1H, NH, D_2O exchangeable); ^{13}C NMR (100 MHz, DMSO-d_6, δ, ppm): 23.8, 45.3, 46.2 (pyrrolidine-Cs), 64.8 (O-$\underline{C}H_2$-C═O), 115.9, 116.2, 128.8, 132.8, 138.7, 151.1 (Ar and olefinic Cs), 158.5, 163.4, 165.0 169.0 (4C═O); Anal. calcd. for $C_{17}H_{17}N_3O_5$; C, 59.47; H, 4.99; N, 12.24; Found; C, 59.70; H, 4.78; N, 12.19.

4.1.2.3. 5-(4-(2-Oxo-2-(piperidin-1-yl)ethoxy)benzylidene)pyrimidine-2,4,6(1H,3H,5H)-trione ***(10c)***. It was prepared from **4a** (0.13 g, 1 mmol) and **9c** (0.25 g, 1 mmol) to give (0.28 g, yield: 78%); m.p. $^{>}$ 300 °C; IR ν (cm^{-1}): 3221 (2NH), 3086 (CH aromatic), 2939 (CH aliphatic), 1743, 1690, 1666 (4C═O); ^{1}H NMR (400 MHz, DMSO-d_6, δ, ppm): 1.12–1.55 (m, 6H, $3CH_2$ piperidine), 3.35–3.41 (m, 4H, N$(CH_2)_2$ piperidine), 4.96 (s, 2H, O-CH_2-C═O), 6.99 (d, J = 8.80 Hz, 2H, ArH), 8.23 (s, 1H, -C═CH–), 8.31 (d, J = 8.80 Hz, 2H, ArH), 11.14 (s, 1H, NH, D_2O exchangeable), 11.27 (s, 1H, NH, D_2O exchangeable); MS, *m/z* [%]: 357.69 [M^+, 46.08]; Anal. calcd. for $C_{18}H_{19}N_3O_5$; C, 60.50; H, 5.36; N, 11.76; Found; C, 60.73; H, 5.48; N, 11.95.

4.1.2.4. 5-(4-(2-Morpholino-2-oxoethoxy)benzylidene)pyrimidine-2,4,6(1H,3H,5H)-trione ***(10d)***. It was prepared from **4a** (0.13 g, 1 mmol) and **9d** (0.25 g, 1 mmol) to give (0.32 g, yield: 90%); m.p. $^{>}$ 300 °C; IR ν (cm^{-1}): 3194, 3132 (2NH), 3062 (CH aromatic), 2966–2924 (CH aliphatic), 1739, 1697, 1661 (4C═O); ^{1}H NMR (400 MHz, DMSO-d_6, δ, ppm): 3.44 (brs, 4H, N$(CH_2)_2$ morpholine), 3.55–3.60 (m, 4H, O$(CH_2)_2$ morpholine), 5.00 (s, 2H, O-CH_2-C═O), 7.01 (d, J = 9.20 Hz, 2H, ArH), 8.23 (s, 1H, -C═CH–), 8.31 (d, J = 8.80 Hz, 2H, ArH), 11.14 (s, 1H, NH, D_2O exchangeable), 11.27 (s, 1H, NH, D_2O exchangeable); ^{13}C NMR (100 MHz, DMSO-d_6, δ, ppm): 45.0 (N$(CH_2)_2$ morpholine), 66.1 (O$(CH_2)_2$ morpholine), 66.5 (O-$\underline{C}H_2$-C═O), 114.6, 116.0, 125.8, 137.6, 138.8, 155.3, 156.0 (Ar and olefinic Cs), 150.7, 162.6, 164.4, 165.9 (4C═O); Anal. calcd. for $C_{17}H_{17}N_3O_6$; C, 56.82; H, 4.77; N, 11.69; Found; C, 56.88; H, 4.91; N, 11.78.

4.1.2.5. 2-(4-((4,6-Dioxo-2-thioxotetrahydropyrimidin-5(2H)ylidene) methyl) phenoxy)-N,N-diethylacetamide ***(11a)***. It was prepared from **4b** (0.14 g, 1 mmol) and **9a** (0.24 g, 1 mmol) to give (0.26 g, yield: 71%); m.p.$^{>}$300 °C; IR ν (cm^{-1}): 3190 (2NH), 3097 (CH aromatic), 2978, 2939 (CH aliphatic), 1690, 1650 (3C═O), 1219 (C═S); ^{1}H NMR (400 MHz, DMSO-d_6, δ, ppm): 1.05–1.23 (m, 6H, $2CH_3$ diethylamine), 3.14–3.30 (m, 4H, $2CH_2$ diethylamine), 4.61 (s, 2H, O-CH_2-C═O), 6.68 (d, J = 8.80 Hz, 2H, ArH), 6.84 (d, J = 8.80 Hz, 2H, ArH), 8.35 (s, 1H, -C═CH-C-), 11.39 (s, 1H, NH, D_2O exchangeable), 11.52 (s, 1H, NH, D_2O exchangeable); ^{13}C NMR (100 MHz, DMSO-d_6, δ, ppm): 14.2, 14.6 ($2CH_3$ diethylamine), 41.1, 41.3 ($2CH_2$ diethylamine), 66.7 (O-CH_2-C═O), 96.4, 114.2, 127.8, 138.0, 156.1 (Ar and olefinic Cs), 164.0, 166.9

(3C═O), 173.05 (C═S); Anal. calcd. for $C_{17}H_{19}N_3O_4S$; C, 56.50; H, 5.30; N, 11.63; Found; C, 56.39; H, 5.48; N, 11.76.

4.1.2.6. 5-(4-(2-Oxo-2-(pyrrolidin-1-yl)ethoxy)benzylidene)-2-thioxodihydro- pyrimidine-4,6(1H,5H)-dione ***(11b)***. It was prepared from **4b** (0.14 g, 1 mmol) and **9b** (0.23 g, 1 mmol) to give (0.27 g, yield: 75%); m.p.>300 °C; IR ν (cm^{-1}): 3113 (2NH), 3062 (CH aromatic), 2970–2927(CH aliphatic), 1697, 1651 (3C═O), 1215 (C═S); ^{1}H NMR (400 MHz, DMSO-d_6, δ, ppm): 1.79–1.92 (m, 4H, $2CH_2$ pyrrolidine), 3.30–3.46 (m, 4H, $N(CH_2)_2$ pyrrolidine), 4.89 (s, 2H, O-CH_2-C═O), 7.07 (d, J = 8.80 Hz, 2H, ArH), 8.25 (s, 1H, -C═CH–), 8.37 (d, J = 8.80 Hz, 2H, ArH), 12.26 (s, 1H, NH, D_2O exchangeable), 12.35 (s, 1H, NH, D_2O exchangeable); Anal. calcd. for $C_{17}H_{17}N_3O_4S$; C, 56.81; H, 4.77; N, 11.69; Found; C, 57.05; H, 4.95; N, 11.48.

4.1.2.7. 5-(4-(2-Oxo-2-(piperidin-1-yl)ethoxy)benzylidene)-2-thioxodihydro- pyrimidine-4,6(1H,5H)-dione ***(11c)***. It was prepared from **4b** (0.14 g, 1 mmol) and **9c** (0.25 g, 1 mmol) to give (0.31 g, yield: 84%); m.p.>300 °C; IR ν (cm^{-1}): 3174 (2NH), 3009 (CH aromatic), 2939 (CH aliphatic), 1675 (3C═O), 1223 (C═S); ^{1}H NMR (400 MHz, DMSO-d_6, δ, ppm): 1.32–1.50 (m, 6H, $3CH_2$ piperidine), 3.25–3.31 (m, 4H, $N(CH_2)_2$ piperidine), 4.63 (s, 2H, O-CH_2-C═O), 6.68 (d, J = 8.80 Hz, 2H, ArH), 6.84 (d, J = 8.80 Hz, 2H, ArH), 8.20 (s, 1H, -C═CH–) 11.39 (s, 1H, NH, D_2O exchangeable), 11.52 (s, 1H, NH, D_2O exchangeable); ^{13}C NMR (100 MHz, DMSO-d_6, δ, ppm): 24.1, 25.6, 26.2 ($3CH_2$ piperidine), 42.9, 45.6 ($N(CH_2)_2$ piperidine), 66.1 (O-$\underline{C}H_2$-C═O), 114.1, 115.5, 127.8, 130.1, 132.3, 151.1 (Ar and olefinic Cs), 163.5, 165.6, 166.6 (3C═O), 192.6 (C═S); MS, *m/z* [%]: 373.18 [M^+, 2.40]; Anal. calcd. for $C_{18}H_{19}N_3O_4S$; C, 57.90; H, 5.13; N, 11.25; Found; C, 58.18; H, 5.32; N, 11.49.

4.1.2.8. 5-(4-(2-Morpholino-2-oxoethoxy)benzylidene)-2-thioxodihydropyrimidine-4,6(1H,5H)-dione ***(11d)***. It was prepared from **4b** (0.14 g, 1 mmol) and **9d** (0.25 g, 1 mmol) to give (0.34 g, yield: 89%); m.p.>300 °C; IR ν (cm^{-1}): 3116 (2NH), 3074 (CH aromatic), 2970–2901 (CH aliphatic), 1700, 1661 (3C═O), 1226 (C═S); ^{1}H NMR (400 MHz, DMSO-d_6, δ, ppm): 3.43 (brs, 4H, $N(CH_2)_2$ morpholine), 3.55–3.61 (m, 4H, $O(CH_2)_2$ morpholine), 5.01 (s, 2H, O-CH_2-C═O), 7.03 (d, J = 8.80 Hz, 2H, ArH), 8.24 (s, 1H, -C═CH-C-), 8.36 (d, J = 8.80 Hz, 2H, ArH), 12.26 (s, 1H, NH, D_2O exchangeable), 12.35 (s, 1H, NH, D_2O exchangeable); ^{13}C NMR (100 MHz, DMSO-d_6, δ, ppm): 41.0 ($N(CH_2)_2$morpholine), 61.5 ($O(CH_2)_2$morpholine), 63.0 (O-$\underline{C}H_2$-C═O), 111.3, 111.9, 128.0, 128.5, 159.1 (Ar and olefinic Cs), 162.0, 166.6 (3C═O), 188.3 (C═S); Anal. calcd. for $C_{17}H_{17}N_3O_5S$; C, 54.39; H, 4.56; N, 11.19; Found; C, 54.62; H, 4.70; N, 11.38.

4.1.2.9. 2-(4-((1,3-Dimethyl-2,4,6-trioxotetrahydropyrimidin-5(2H)-ylidene)methyl) phenoxy)-N,N-diethylacetamide ***(12a)***. It was prepared from **4c** (0.16 g, 1 mmol) and **9a** (0.24 g, 1 mmol) to give (0.26 g, yield: 71%); m.p. > 300 °C; IR ν (cm^{-1}): 3082–3047 (CH aromatic), 2970–2935 (CH aliphatic), 1728, 1666 (4C═O); ^{1}H NMR (400 MHz, $CDCl_3$, δ, ppm): 1.13–1.25 (m, 6H, $2CH_3$ of diethylamine), 3.31–3.42 (m, 10*H*, 2 N-CH_3 + $2CH_2$ of diethylamine), 4.78 (s, 2H, O-CH_2-C═O), 7.02 (d, J = 8.80 Hz, 2H, ArH), 8.30 (d, J = 8.80 Hz, 2H, ArH), 8.50 (s, 1H, -C═CH-C-); Anal. calcd. for $C_{19}H_{23}N_3O_5$; C, 61.12; H, 6.21; N, 11.25; Found; C, 61.40; H, 6.34; N, 11.49.

4.1.2.10. 1,3-Dimethyl-5-(4-(2-oxo-2-(pyrrolidin-1-yl)ethoxy) benzylidene) pyrimidine-2,4,6 (1H,3H,5H)-trione ***(12b)***. It was prepared from **4c** (0.16 g, 1 mmol) and **9b** (0.23 g, 1 mmol) to give (0.28 g, yield: 75%); m.p.>300 °C; IR ν (cm^{-1}): 3078 (CH aromatic), 2951 (CH aliphatic), 1732, 1680, 1661 (4C═O); ^{1}H NMR (400 MHz, $CDCl_3$, δ, ppm): 1.87–1.99 (m, 4H, $2CH_2$ pyrrolidine), 3.38 (s, 3H, N-CH_3), 3.41 (s, 3H, N-$\underline{C}H_3$), 3.51–3.53 (m, 4H, $N(CH_2)_2$ pyrrolidine), 4.72 (s, 2H, O-CH_2-C═O), 7.01 (d, J = 8.80 Hz, 2H, ArH), 8.28 (d, J = 8.80 Hz, 2H, ArH), 8.49 (s, 1H, -C═CH-C-); ^{13}C NMR (100 MHz, DMSO-d_6, δ, ppm): 23.8, 25.9 ($2CH_2$pyrrolidine), 28.3 ($2CH_3$), 45.3, 46.2 ($N(CH_2)_2$ pyrrolidine), 66.2 (O-$\underline{C}H_2$-C═O), 110.0, 114.8, 115.5, 130.1, 132.3, 137.3 (Ar and olefinic Cs), 156.7, 163.5, 165.0, 166.0 (4C═O); Anal. calcd. for $C_{19}H_{21}N_3O_5$; C, 61.45; H, 5.70; N, 11.31; Found; C, 61.38; H, 5.87; N, 11.43.

4.1.2.11. 1,3-Dimethyl-5-(4-(2-oxo-2-(piperidin-1-yl)ethoxy)benzylidene) pyrimidine-2,4,6 (1H,3H,5H)-trione ***(12c)***. It was prepared from **4c** (0.16 g, 1 mmol) and **9c** (0.25 g, 1 mmol) to give (0.32 g, yield: 82%); m.p. > 300 °C; IR ν (cm^{-1}): 3066 (CH aromatic), 2939 (CH aliphatic), 1728, 1666 (4C═O); ^{1}H NMR (400 MHz, $CDCl_3$, δ, ppm): 1.57–1.66 (m, 6H, $3CH_2$ piperidine), 3.38 (s, 3H, N-CH_3), 3.41 (s, 3H, N-CH_3), 3.48–3.54 (m, 4H, $N(CH_2)_2$ piperidine), 4.78 (s, 2H, O-CH_2-C═O), 7.02 (d, J = 8.80 Hz, 2H, ArH), 8.29 (d, J = 8.80 Hz, 2H, ArH), 8.50 (s, 1H, -C═CH–); ^{13}C NMR (100 MHz, DMSO-d_6, δ , ppm): 24.3, 25.5, 26.4 ($3CH_2$ piperidine), 28.9, 29.0 ($2CH_3$), 43.1, 46.1 ($N(CH_2)_2$ piperidine), 67.0 (O-$\underline{C}H_2$-C═O), 114.6, 115.9, 124.2, 137.6, 138.7, 158.0, 158.8 (Ar and olefinic Cs), 151.4, 160.8, 162.6, 164.9 (4C═O); Anal. calcd. for $C_{20}H_{23}N_3O_5$; C, 62.33; H, 6.02; N, 10.90; Found; C, 62.19; H, 6.29; N, 11.13.

4.1.2.12. 1,3-Dimethyl-5-(4-(2-morpholino-2-oxoethoxy)benzylidene) pyrimidine-2,4,6(1H,3H,5H)-trione ***(12d)***. It was prepared from **4c** (0.16 g, 1 mmol) and **9d** (0.25 g, 1 mmol) to give (0.36 g, yield: 92%); m.p. > 300 °C; IR ν (cm^{-1}): 3066–3047 (CH aromatic), 2962 (CH aliphatic), 1724, 1666 (4C═O); ^{1}H NMR (400 MHz, $CDCl_3$, δ, ppm): 3.39 (s, 3H, N-CH_3), 3.41 (s, 3H, N-CH_3), 3.58–3.60 (m, 4H, $N(CH_2)_2$ morpholine), 3.67–3.71 (m, 4H, $O(CH_2)_2$ morpholine), 4.79 (s, 2H, O-CH_2-C═O), 7.02 (d, J = 8.80 Hz, 2H, ArH), 8.28 (d, J = 8.80 Hz, 2H, ArH), 8.50 (s, 1H, -C = CH–); MS, *m/z* [%]: 387.00 [M^+, 45.65]; Anal. calcd. for $C_{19}H_{21}N_3O_6$; C, 58.91; H, 5.46; N, 10.85; Found; C, 58.74; H, 5.41; N, 10.98.

4.2. Biological evaluation

4.2.1. PARP1 inhibitory activity assay

PARP1 enzyme inhibition activity was measured for the tested compounds using a colorimetric 96-well PARP1 assay kit (BPS Bioscience) (catalog no. 80580), according to the manufacturer's protocol. Briefly, the histone mixture was diluted 1:5 with 1 × PBS, 50 µl of histone solution was added to each well and incubated at 4 °C overnight. The plate was washed three times using 200 µl PBST buffer (1 × PBS containing 0.05% Tween-20) per well. Liquid was removed from the wells by tapping the strip wells on clean paper towels. To each well, 200 µl of blocking buffer was added, followed by 60–90 min. incubation at room temperature. Then 25 µl of PARP master mixture (consisting of (2.5 µl 10× PARP buffer + 2.5 µl 10× PARP Assay mixture + 5 µl activated DNA + 15 µl distilled water) was added to each well. AZD2281 (Olaparib) was used as a positive control. 5 µl of Inhibitor solution of each well labeled as "Test Inhibitor" was added. For the "Positive Control" and "Blank", 5 µl of the same solution without inhibitor was added. 1x PARP buffer was prepared by adding 1 part of 10x PARP buffer to 9 parts H_2O (v/v), 20 µl of 1x PARP buffer was added to the wells designated as "Blank". The amount of PARP1 required for the assay was then calculated. The reaction was initiated by adding 20 µl of diluted PARP1 enzyme to the wells designated "Positive Control" and "Test Inhibitor Control". The strip wells were incubated at room temperature for 1 h. The strip wells were then washed three times with 200 µl PBST buffer. Then, 50 µl of 50 times diluted Streptavidin-HRP with blocking buffer was added to each well, and the strips were further incubated at room temperature for 30 min. After washing the wells three times with 200 µl PBST buffer, HRP colorimetric substrate was added to each well and the plate was incubated at the room temperature until a blue color is developed in the positive control well. Then reaction was quenched with 100 ml/well of 2 M sulfuric acid, and absorbance at 450 nm was determined. Carrier solvents were assayed as

negative controls. All assays were performed in triplicate. To determine the IC_{50} value for each inhibitor, the average absorbance of each inhibitor concentration was plotted against the log of the concentration of each respective inhibitor and the IC_{50} value for each plot was obtained using computer-assisted non-linear regression analyses. Data presented are the results of at least two independent experiments done in triplicate.

4.2.1.1. NCI-60 human tumor cell lines screen. All the compounds were selected for NCI-60 Human Tumor Cell Lines Screen by the Developmental Therapeutics Program (DTP) at the National Cancer Institute (NCI), Maryland, USA. The compounds were supplied as dry powder and a single concentration is tested in all 60 cell lines at a single dose of 10 μM solution in dimethyl sulfoxide (DMSO) using Sulforhodamine B assay. Briefly, cells are seeded in 96 well plates at an appropriate density and incubated for 1 day. After 1 day, some of the plates are processed to determine the density time zero. To the remaining plates, compounds are added at 10 μM concentration. Plates are incubated a further 2 days, then fixed and stained with sulphorhodamine B. Growth inhibition is calculated relative to cells without drug treatment and the time zero control. The use of a time zero control allows the determination of cell kill as well as net growth inhibition.

4.2.1.2. Antiproliferative activity against BRCA mutated cell line MDA-MB-436. Antiproliferative activity of **5c, 7b, 7d, 7e, 12a** and **12c** in MDA-MB-436 cell line was measured spectrophotometrically using *in vitro* MTT based toxicology assay kit (catalog no. M-5655, M-8910) (Sigma Aldrich), according to the manufacturer's protocol. Briefly, cells were platted (cells density 1.2 – 1.8 × 10,000 cells/well) in a volume of 100 μl complete growth medium + 100 μl of the tested compound per well in a 96-well plate for 48 h before the MTT assay. The cultures were removed from incubator into laminar flow hood then each vial of MTT [M-5655] should be reconstituted with 3 ml of medium or balanced salt solution without phenol red and serum. Reconstituted MTT was added in an amount equal to 10% of the culture medium volume. Cultures were returned to incubator for 2–4 h. After the incubation period, cultures were removed from incubator and the resulting formazan crystals were dissolved by adding an amount of MTT solubilization solution [M-8910] equal to the original culture medium volume. Dissolution is enhanced by gentle mixing in a gyratory shaker. Then the absorbance is measured spectrophotometrically at a wavelength of 450 nm. The absorbance of multiwell plates was measured at 690 nm and subtracted from the 450 nm measurement. To determine the IC_{50} value for each inhibitor, the average absorbance of each inhibitor concentration was plotted against the log of the concentration of each respective inhibitor and the IC_{50} value for each plot was obtained using computer-assisted non-linear regression analyses. Data presented are the results of at least two independent experiments done in triplicate. The results of these studies are presented as mean IC_{50} (μM) ± standard deviation (SD).

4.2.1.3. Cell cycle analysis in MDA-MB-436 cells and apoptotic effects. Annexin V-FITC Apoptosis Detection Kit (BioVision) was used to determine the effect of **5c** and **12c** on the cell cycle profile of MDA-MB-436 according to the manufacturer procedure. BD FACSCalibur flow cytometer was used for detection of the results at 48 h.

4.2.1.4. Potentiation of temozolomide antiproliferative activity in A549 human lung cancer cells. Cells were obtained from American Type Culture Collection. Cells were cultured using DMEM (Invitrogen/Life Technologies) supplemented with 10% FBS (Hyclone), 10 ug/ml of insulin (Sigma), and 1% penicillin–streptomycin. All the other chemicals and reagents were from Sigma, or Invitrogen. The protocol similar to the one used in MTT assay in MDA-MB-436 cell line.

4.3. Molecular docking study

The parameters of Amber10:EHT forcefield in MOE was selected for potential setup. Amber10:EHT forcefield uses the following parameters: AMBER parameters for proteins and nucleic acids (ff10), EHT parameters for small molecules, AM1-BCC charges are expected for small molecules and Group II ion and Group VIII parameters from OPLS-AA. The X-ray crystal structure of Olaparib in complex with PARP1 (PDB: 5DS3) was downloaded from Protein Data Bank available at http://www.rcsb.org/pdb in PDB format [30].The protein–ligand complex was prepared by removal of water of crystallization, two sulphate ions and one polyethylene glycol (PEG) that were not involved in the binding. Protonation of the crystal structure was performed, where hydrogen atoms were added at their standard geometry, the partial charges were computed, and the system was optimized using "QuickPrep" preparation protocol in MOE. Isolation of the active site and recognition of the involved amino acids was carried out using "Site View" tool. The 2D interaction diagram of the co-crystallized ligand (Olaparib) and PARP1 was isolated using "Ligand Interactions" tool in MOE. The compounds were built using ChemBioDraw Ultra 19.0 and their SMILES were copied to MOE. 3D Protonation of the compounds was carried out using the precise mode in "Protonate" tool and the most prevalent ionized form was selected for subsequent steps. Energy minimization of the structures using 10:EHT forcefield and a gradient of 0.05 was applied using "Energy Minimize" tool. The partial charges were automatically calculated for each molecule. Conformational analysis was run using the default settings for systematic search. The least energy conformer of each molecule was saved to another data base to be docked into the catalytic domain of PARP1. Docking of the least energy conformers was performed by definition of the receptor atoms as (receptor) and site of placement was defined as (ligand atoms). The database containing the least energy conformers of the target compounds was used as the input for the docking procedure. Placement method was adjusted to (triangle matcher). Rescoring method was adjusted to (London dG). Finally, the docking poses were examined for protein ligand-interactions and the docking scores were recorded.

Declaration of Competing Interest

The authors declare that they have no known competing financial interests or personal relationships that could have appeared to influence the work reported in this paper.

Acknowledgement

The authors are thankful for the members of the Developmental Therapeutics Program (DTP) at the National cancer Institute (NCI), Maryland, USA for performing the NCI-60 Human Tumor Cell Lines Screen.

Appendix A. Supplementary material

Supplementary data to this article can be found online at https://doi.org/10.1016/j.bioorg.2020.104198.

References

[1] J.C. Ame, C. Spenlehauer, G. de Murcia, The PARP superfamily, BioEssays 26 (8) (2004) 882–893.
[2] Y. Wang, N.S. Kim, J.-F. Haince, H.C. Kang, K.K. David, S.A. Andrabi, G.G. Poirier, V.L. Dawson, T.M.J.S.S. Dawson, Poly (ADP-ribose)(PAR) binding to apoptosis-inducing factor is critical for PAR polymerase-1–dependent cell death (parthanatos), Sci. Signal 4 (167) (2011) pp. ra20-ra20.
[3] J. Morales, L. Li, F.J. Fattah, Y. Dong, E.A. Bey, M. Patel, J. Gao, D.A. Boothman, Review of poly (ADP-ribose) polymerase (PARP) mechanisms of action and rationale for targeting in cancer and other diseases, Crit. Rev. Eukaryot. Gene Expr. 24 (1) (2014) 15–28.
[4] D.V. Ferraris, Evolution of poly(ADP-ribose) polymerase-1 (PARP-1) inhibitors.

From concept to clinic, J. Med. Chem. 53 (12) (2010) 4561–4584.
[5] C.J. Lord, A. Ashworth, The DNA damage response and cancer therapy, Nature 481 (7381) (2012) 287–294.
[6] B.W. Durkacz, O. Omidiji, D.A. Gray, S. Shall, (ADP-ribose)n participates in DNA excision repair, Nature 283 (5747) (1980) 593–596.
[7] D.A. Loser, A. Shibata, A.K. Shibata, L.J. Woodbine, P.A. Jeggo, A.J. Chalmers, Sensitization to radiation and alkylating agents by inhibitors of poly(ADP-ribose) polymerase is enhanced in cells deficient in DNA double-strand break repair, Mol. Can. Ther. 9 (6) (2010) 1775–1787.
[8] M.E. Moynahan, M.J.N.r.M.c.b. Jasin, Mitotic homologous recombination maintains genomic stability and suppresses tumorigenesis, Nat Rev Mol Cell Biol, 11(3) (2010) 196–207.
[9] M.R.J.N.s. Lieber, m. biology, NHEJ and its backup pathways in chromosomal translocations, Nat Struct Mol Biol, 17(4) (2010) 393–395.
[10] K. Yoshida, Y. Miki, Role of BRCA1 and BRCA2 as regulators of DNA repair, transcription, and cell cycle in response to DNA damage, Cancer Sci 95 (11) (2004) 866–871.
[11] W.K. Holloman, Unraveling the mechanism of BRCA2 in homologous recombination, Nat. Struct. Mol. Biol. 18 (7) (2011) 748–754.
[12] H. Farmer, N. McCabe, C.J. Lord, A.N.J. Tutt, D.A. Johnson, T.B. Richardson, M. Santarosa, K.J. Dillon, I. Hickson, C. Knights, N.M.B. Martin, S.P. Jackson, G.C.M. Smith, A. Ashworth, Targeting the DNA repair defect in BRCA mutant cells as a therapeutic strategy, Nature 434 (7035) (2005) 917–921.
[13] H.E. Bryant, N. Schultz, H.D. Thomas, K.M. Parker, D. Flower, E. Lopez, S. Kyle, M. Meuth, N.J. Curtin, T. Helleday, Specific killing of BRCA2-deficient tumours with inhibitors of poly(ADP-ribose) polymerase, Nature 434 (7035) (2005) 913–917.
[14] P.C. Fong, D.S. Boss, T.A. Yap, A. Tutt, P. Wu, M. Mergui-Roelvink, P. Mortimer, H. Swaisland, A. Lau, M.J. O'Connor, A. Ashworth, J. Carmichael, S.B. Kaye, J.H. Schellens, J.S. de Bono, Inhibition of poly(ADP-ribose) polymerase in tumors from BRCA mutation carriers, N Engl. J. Med. 361 (2) (2009) 123–134.
[15] S.K. Pal, J. Mortimer, Triple-negative breast cancer: novel therapies and new directions, Maturitas 63 (4) (2009) 269–274.
[16] G. O'Sullivan Coyne, A.P. Chen, R. Meehan, J.H. Doroshow, PARP inhibitors in reproductive system cancers: current use and developments, Drugs 77 (2) (2017) 113–130.
[17] Z. Yuan, J. Chen, W. Li, D. Li, C. Chen, C. Gao, Y. Jiang, PARP inhibitors as antitumor agents: a patent update (2013–2015), Expert. Opin. Ther. Pat. 27 (3) (2017) 363–382.
[18] Y.Q. Wang, P.Y. Wang, Y.T. Wang, G.F. Yang, A. Zhang, Z.H. Miao, An update on poly(ADP-ribose)polymerase-1 (PARP-1) inhibitors: opportunities and challenges in cancer therapy, J. Med. Chem. 59 (21) (2016) 9575–9598.
[19] A. Mullard, PARP inhibitors plough on, Nat. Rev. Drug. Discov. 16 (4) (2017) 229.
[20] K.Y. Lin, W.L. Kraus, PARP inhibitors for cancer therapy, Cell 169 (2) (2017) 183.
[21] FDA approves PARP inhibitor for ovarian cancer, Nat. Biotechnol. 35(5) (2017) 398.
[22] J. Zhou, M. Ji, Z. Zhu, R. Cao, X. Chen, B. Xu, Discovery of 2-substituted 1H-benzo[d]immidazole-4-carboxamide derivatives as novel poly(ADP-ribose)polymerase-1 inhibitors with in vivo anti-tumor activity, Eur. J. Med. Chem. 132 (2017) 26–41.
[23] N. Chadha, O. Silakari, Identification of low micromolar dual inhibitors for aldose reductase (ALR2) and poly (ADP-ribose) polymerase (PARP-1) using structure based design approach, Bioorg. Med. Chem. Lett. 27 (11) (2017) 2324–2330.
[24] X. Chen, X. Huan, Q. Liu, Y. Wang, Q. He, C. Tan, Y. Chen, J. Ding, Y. Xu, Z. Miao, C. Yang, Design and synthesis of 2-(4,5,6,7-tetrahydrothienopyridin-2-yl)-benzoimidazole carboxamides as novel orally efficacious Poly(ADP-ribose)polymerase (PARP) inhibitors, Eur. J. Med. Chem. 145 (2018) 389–403.
[25] Y. Zhong, Y. Meng, X. Xu, L. Zhao, Z. Li, Q. You, J. Bian, Design, synthesis and evaluation of phthalazinone thiohydantoin-based derivative as potent PARP-1 inhibitors, Bioorg. Chem. 91 (2019) 103181.
[26] J. Zhou, M. Ji, H. Yao, R. Cao, H. Zhao, X. Wang, X. Chen, B. Xu, Discovery of quinazoline-2,4(1H,3H)-dione derivatives as novel PARP-1/2 inhibitors: design, synthesis and their antitumor activity, Org. Biomol. Chem. 16 (17) (2018) 3189–3202.
[27] G.F. Elmasry, E.E. Aly, F.M. Awadallah, S.M. El-Moghazy, Design and synthesis of novel PARP-1 inhibitors based on pyridopyridazinone scaffold, Bioorg. Chem. 87 (2019) 655–666.
[28] D.K. Nilov, K.I. Yashina, I.V. Gushchina, A.L. Zakharenko, M.V. Sukhanova, O.I. Lavrik, V.K. Svedas, 2,5-Diketopiperazines: A new class of poly(ADP-ribose) polymerase inhibitors, Biochemistry (Mosc) 83 (2) (2018) 152–158.
[29] T. Eltze, R. Boer, T. Wagner, S. Weinbrenner, M.C. McDonald, C. Thiemermann, A. Burkle, T. Klein, Imidazoquinolinone, imidazopyridine, and isoquinolindione derivatives as novel and potent inhibitors of the poly(ADP-ribose) polymerase (PARP): a comparison with standard PARP inhibitors, Mol. Pharmacol. 74 (6) (2008) 1587–1598.
[30] J.M. Dawicki-McKenna, M.F. Langelier, J.E. DeNizio, A.A. Riccio, C.D. Cao, K.R. Karch, M. McCauley, J.D. Steffen, B.E. Black, J.M. Pascal, PARP-1 activation requires local unfolding of an autoinhibitory domain, Mol. Cell 60 (5) (2015) 755–768.
[31] M.J.T.J.o.P.C. Krahl, The effect of variation in ionic strength and temperature on the apparent dissociation Cconstants of thirty substituted barbituric acids, J Phys Chem, 44(4) (1940), pp. 449-463.
[32] U. Schatzschneider, T. Weyhermüller, E.J.E.J.o.I.C. Rentschler, Metal Complexes with Nitronyl Nitroxide Substituted Phenolate Ligands Providing New Magnetic Exchange Interaction Pathways − Synthesis, Structures, Magnetic Dilution Studies, and Ab Initio Calculations, Eur. J. Inorg. Chem., 2001(10) (2001), pp. 2569-2586.
[33] J. Dickey, A. Gray, Barbituric acid, Organic Syntheses, 18 (2003), pp. 8-8.
[34] M.R. Patel, A. Bhatt, J.D. Steffen, A. Chergui, J. Murai, Y. Pommier, J.M. Pascal, L.D. Trombetta, F.R. Fronczek, T.T. Talele, Discovery and structure-activity relationship of novel 2,3-dihydrobenzofuran-7-carboxamide and 2,3-dihydrobenzofuran-3(2H)-one-7-carboxamide derivatives as poly(ADP-ribose)polymerase-1 inhibitors, J. Med. Chem. 57 (13) (2014) 5579–5601.
[35] O.N. Ikediobi, H. Davies, G. Bignell, S. Edkins, C. Stevens, S. O'Meara, T. Santarius, T. Avis, S. Barthorpe, L. Brackenbury, G. Buck, A. Butler, J. Clements, J. Cole, E. Dicks, S. Forbes, K. Gray, K. Halliday, R. Harrison, K. Hills, J. Hinton, C. Hunter, A. Jenkinson, D. Jones, V. Kosmidou, R. Lugg, A. Menzies, T. Mironenko, A. Parker, J. Perry, K. Raine, D. Richardson, R. Shepherd, A. Small, R. Smith, H. Solomon, P. Stephens, J. Teague, C. Tofts, J. Varian, T. Webb, S. West, S. Widaa, A. Yates, W. Reinhold, J.N. Weinstein, M.R. Stratton, P.A. Futreal, R. Wooster, Mutation analysis of 24 known cancer genes in the NCI-60 cell line set, Mol. Can. Ther. 5 (11) (2006) 2606–2612.
[36] B. Stordal, K. Timms, A. Farrelly, D. Gallagher, S. Busschots, M. Renaud, J. Thery, D. Williams, J. Potter, T. Tran, G. Korpanty, M. Cremona, M. Carey, J. Li, Y. Li, O. Aslan, J.J. O'Leary, G.B. Mills, B.T. Hennessy, BRCA1/2 mutation analysis in 41 ovarian cell lines reveals only one functionally deleterious BRCA1 mutation, Mol. Oncol. 7 (3) (2013) 567–579.
[37] F. Elstrodt, A. Hollestelle, J.H.A. Nagel, M. Gorin, M. Wasielewski, A. van den Ouweland, S.D. Merajver, S.P. Ethier, M. Schutte, BRCA1 mutation analysis of 41 human breast cancer cell lines reveals three new deleterious mutants, Can. Res. 66 (1) (2006) 41.
[38] Y. Shi, F. Zhou, F. Jiang, H. Lu, J. Wang, C. Cheng, PARP inhibitor reduces proliferation and increases apoptosis in breast cancer cells, Chin. J. Can. Res. 26 (2) (2014) 142–147.
[39] T.J. Gaymes, S. Shall, L.J. MacPherson, N.A. Twine, N.C. Lea, F. Farzaneh, G.J. Mufti, Inhibitors of poly ADP-ribose polymerase (PARP) induce apoptosis of myeloid leukemic cells: potential for therapy of myeloid leukemia and myelodysplastic syndromes, Haematologica 94 (5) (2009) 638–646.
[40] H. Wang, S. Zhang, L. Song, M. Qu, Z. Zou, Synergistic lethality between PARP-trapping and alantolactone-induced oxidative DNA damage in homologous recombination-proficient cancer cells, Oncogene 39 (14) (2020) 2905–2920.
[41] H.C. Chuang, N. Kapuriya, S.K. Kulp, C.S. Chen, C.L. Shapiro, Differential anti-proliferative activities of poly(ADP-ribose) polymerase (PARP) inhibitors in triple-negative breast cancer cells, Breast Can. Res Treat. 134 (2) (2012) 649–659.
[42] A. Pierce, P.M. McGowan, M. Cotter, M. Mullooly, N. O'Donovan, S. Rani, L. O'Driscoll, J. Crown, M.J. Duffy, Comparative antiproliferative effects of iniparib and olaparib on a panel of triple-negative and non-triple-negative breast cancer cell lines, Can. Biol. Ther. 14 (6) (2013) 537–545.
[43] I. Campillo-Marcos, P.A. Lazo, Olaparib and ionizing radiation trigger a cooperative DNA-damage repair response that is impaired by depletion of the VRK1 chromatin kinase, J. Exp. Clin. Can. Res. 38 (1) (2019) 203.
[44] S. Li, X.Y. Li, T.J. Zhang, J. Zhu, W.H. Xue, X.H. Qian, F.H. Meng, Design, synthesis and biological evaluation of erythrina derivatives bearing a 1,2,3-triazole moiety as PARP-1 inhibitors, Bioorg Chem 96 (2020) 103575.
[45] J.M. Senra, B.A. Telfer, K.E. Cherry, C.M. McCrudden, D.G. Hirst, M.J. O'Connor, S.R. Wedge, I.J. Stratford, Inhibition of PARP-1 by olaparib (AZD2281) increases the radiosensitivity of a lung tumor xenograft, Mol. Can. Ther. 10 (10) (2011) 1949–1958.